이학박사학위논문

Development of Signal-Responsive Materials and Their Application of Osmotic Control and Desalination

신호감응성 물질 개발과 이를 이용한 삼투 조절

2016년 8월

서울대학교 대학원
화학부 생화학전공

목 영 봉

Abstract

Stimuli-responsive molecules responding to small changes in the environmental condition are elemental components consisting of so-called functional smart materials. Among physical stimuli described above, a temperature change as a stimulus and relating thermoresponsive molecules have been the most widely studied because of the easiness for stimulation and the effectiveness after stimulation. Thermoresponsive molecules show either lower critical solution temperature (LCST) or upper critical solution temperature (UCST) phase transition phenomenon. LCST molecules are soluble in certain solvents at low temperature and show abrupt phase separation above certain temperature points. Oppositely, UCST molecules are soluble in the solvents at higher temperature and phase-separate below certain temperature points.

Thermoresponsive molecules showing L/UCST phenomena in water have been widely applied in material and medical sciences. However, most thermoresponsive molecules are polymeric having high molecular weight (MW) values because low MW ones have large positive statistical entropy of mixing which would result easy solubilization in water at observable temperature condition. These features limit significant changes in the effective molar concentration and might have restricted the corresponding applications. Moreover, introduction of another remote-controllable stimulus into pre-existing thermoresponsive molecules would result in more delicate signal responsiveness.

In this dissertation, I demonstrate that nonpolymeric small molecules derived from thermoresponsive polymers show thermoresponsiveness owing to compensated increase in hydrophobicity. Next, I introduce light-tunable thermoresponsive molecules for effective remote control of L/UCSTs in water. Finally, I show control of osmosis based on aqueous solution of small LCST molecules realized by remarkable change in effective concentration upon temperature changes.

Branched polyethylenimine (*b*-PEI) molecules were acylated and the resultant *b*-PEI derivatives showed LCST phenomena. Small molecules derived from the structure of acylated *b*-PEIs (LCST polymers) showed LCST phenomena in water. As an expansion of the chemical structure of small LCST molecules, thermoresponsiveness of glycol ethers was also studied.

Next, light-modulated shifts in aqueous L/UCSTs were observed after introduction of azobenzene moieties into pre-existing *b*-PEI derivatives showing L/UCSTs. Especially, the largest shifts in LCST after irradiation over previous reports were observed and light-induced alternation of UCST in water was demonstrated for the first time.

Finally, control of osmosis was demonstrated by small LCST molecules at high concentration. Aqueous solution of the synthesized LCST molecules showed high osmotic pressure at low temperature and it was abruptly decreased after phase separation at higher temperature. The change in osmotic pressures resulted in osmotic flow changes at different temperatures. By using this

phenomenon, continuous osmotic desalination process was demonstrated. In this process two osmotic flows at different temperatures are linked and higher saline solution could be replaced to weak saline solution. This process is expected to be developed as a novel desalination process.

I hope the demonstration described in this dissertation to become expansion of academic understandings of MW-thermoresponse relationships and multi-stimuli responsiveness, and basis for research and development of osmotic desalination.

Keywords: Thermoresponsive molecules, lower critical solution temperature (LCST), upper critical solution temperature (UCST) azobenzene, osmosis, desalination.

Student Number: 2010-23088

Table of Contents

Part II. Photoisomerization-Induced Modulation of Lower and Upper Critical Solution Temperature Phase Transition Behavior of Branched Polyethylenimine Derivatives in Water

List of Figures

Part I. Development of Lower Critical Solution Temperature Phase Transition Materials with Decreased Molecular Weight

Part II. Photoisomerization-Induced Modulation of Lower and Upper Critical Solution Temperature Phase Transition Behavior of Branched Polyethylenimine Derivatives in Water

Part III. Control of Osmosis and Desalination Driven by Lower Critical Solution Temperature Phase Transition Materials

Chapter 1. Contorl of Osmosis and Circulatory Desalination Based on *N*-Butyrylated Amine Derivatives

Chapter 2. Forward Osmotic Contorl Driven by Glycol Ethers

List of Tables

Chapter 2. Forward Osmotic Contorl Driven by Glycol Ethers

Part I. Development of Lower Critical Solution Temperature Phase Transition Materials with Decreased Molecular Weight

1. Introduction

Due to the recent rapid growth of biological and medical uses of polymers, the application of smart polymers whose physicochemical properties change in response to biosignals such as ionic concentration, pH, glutathione concentration, light, and temperature change are being increasingly developed.[1,2] Among the biosignals, physical signals including light and temperature change are easily controllable. For example, temperature change, which may be induced by inflammation or activated metabolism in a biosystem, can also be generated externally by a heat pad or illumination.[3] The time- and site-specific control of a physical signal will attract considerable attention to temperature-responsive polymers considering that the variety of light-responsive polymers is still limited.

Most temperature-responsive polymers, also known as thermoresponsive polymers, show a hydrophilic to hydrophobic phase transition above a certain temperature known as the lower critical solution temperature (LCST). Due to the negative entropy change (ΔS_{mix}) during the solvation of thermoresponsive polymers, they form insoluble aggregates in aqueous solutions when the Gibbs free energy of hydration ($\Delta G_{mix} = \Delta H_{mix} - T\Delta S_{mix}$) becomes positive above the LCST at certain mole fraction assuming that temperature dependence of enthalpy and entropy is neglected.[4]

After the LCST transition of poly(*N*-isopropylacrylamide) (PNIPAAM) was discovered [5], the thermoresponsivity of other

poly (N-substituted acrylamide)s [6], poly(N-alkyloxazoline)s [7], amphiphilic block copolymers [8], and polypeptides [9], has been intensively investigated. Of course, polymers that show a LCST transition in the biologically tolerable temperature range of 20-40 °C are more attractive for biomedical uses such as in hydrogel [10], tissue engineering [11], and drug/gene delivery [12] applications.

Since the concentration of the solution is dramatically decreased after phase separation, the LCST transition can also be applied to the thermoresponsive control of concentration gradients. However, most thermoresponsive materials are polymeric molecules which cannot obtain higher molar concentration and higher composition.

Statistical entropy of mixing of smaller molecules is larger than that of higher MW molecules. Thus overall entropy of mixing of smaller molecules should be higher than that of corresponding larger molecule regarding that they have similar molecular structure, *i.e.* same repeating units but different MWs. Because increase in the entropy of mixing (negative value) is equal to decrease in absolute value of the entropy of mixing, the phase transition temperature should be increased. Therefore, it is hard to observe phase transition at normal condition (0-100 °C) if the MW is significantly lowered. To compensate the increased ΔS, hydrophobicity of the molecule should be increased because increased hydrophobic moiety results more negative ΔS_{mix} originated from more ordered water.

In this part, small thermoresponsive materials derived from the pre-existing polymers are introduced. Higher solubility in water and large difference in effective concentration are highlighted.

2. Experimental Details

2.1. Preparation of thermoresponsive molecules

Tris(2-aminoethyl)amine (TAEA, purchased from Sigma-Aldrich, USA) (30 mL, 200 mmol) or branched polyethylenimine (*b*-PEI) (purchased from Sigma-Aldrich, M_n = 600, M_w = 800) (50 g, 84 mmol) was dissolved in 400 mL 1 M $NaHCO_3$ with 400 mL methanol. *n*-butyric anhydride (purchased from TCI chemicals, Japan, 125.88 mL, 800 mmol) was slowly added to the solution at 0 ℃ with vigorous stirring. After 1 h of stirring at 0 ℃, the solution was further stirred for 18 h at ambient temperature. The reaction mixture was adjusted to about pH 11 by addition of 1 M NaOH, and extracted with methylene chloride (×3). The organic extract was dried with $MgSO_4$, and evaporated under vacuum to produce the final products, *N,N',N"*-tri(*n*-butyrylated) tris(2-aminoethyl)amine (*n*Bu-TAEA) as a white solid (> 70 g, > 98% yield), and *n*-butyrylated polyethylenimine (*n*Bu-PEI) as a pale yellow viscous liquid (> 100 g, > 96% yield). Di(ethylene glycol) *n*-hexyl ether (DEH) and propylene glycol *n*-butyl ether (PB) were purchased from Sigma-Aldrich, USA. Di(propylene glycol) *n*-propyl ether (DPP) was kindly donated from Dow Chemical, USA.

2.2. Measurements of LCST phase transition

The LCST phase transition of solutions containing thermoresponsive solutes was measured by a UV-Vis

spectrophotometer at a wavelength of 600 nm. To determine the phase transition temperature, transmittance was measured by increasing the temperature. The phase transition temperature was defined as that temperature at which the transmittance was below 95%.

2.3. Compositions of *n*Bu-PEI and *n*Bu-TAEA in the water-rich phase after phase separation

Concentrations of water-rich phases of *n*Bu-TAEA and *n*Bu-PEI solution after phase separation at 55 ° C were measured by ^{1}H-NMR. To measure the concentrations of water-rich phases, I prepared internal standard calibrations. Acetic acid was used as internal standard. I made calibration curve measuring ^{1}H-NMR integration ratio of precisely-made LCST draw solution at various concentrations comparing with that of the constant concentration of acetic acid. Then concentrations of LCST draw solutes in the water-rich phase at 55 ° C were determined.

2.4. Concentrations of the GE-rich phase and water-rich phase following phase separation

The concentrations of the GE-rich phase and water-rich phase following phase separation at 30 ° C, 40 ° C, and 50 ° C were measured by ^{1}H-NMR. After a 1 hour relaxation of 30 w/w % (weight of GE / weight of GE and water) GE solutions at each temperature in an oil bath, the GE-rich phase and water-rich phase

were carefully collected in a glass tube. The concentration of the GE in each phase was determined by $^{1}H-NMR$ using a set quantity of acetic acid as an internal standard.

3. Results and Discussion

3.1. Synthesis of thermoresponsive molecules

I prepared LCST materials, *n*Bu-PEI and *n*Bu-TAEA, by a simple one-step synthetic method (Fig. 1). Inspired by the molecular structures of poly(*N*-substituted acrylamide)s[13] and poly(*N*-alkyloxazoline)s,[14] the introduction of hydrophobic acyl groups into amine groups is an economical method of synthesizing thermoresponsive materials. The phase transition temperature and aqueous solubility are controlled by the hydrophobicity of the acyl moieties. As the hydrophobicity of the acyl moieties increases, both phase transition temperature and aqueous solubility decrease. Between low phase transition temperature and high aqueous solubility, I chose a 4-carbon *n*-butyryl (*n*Bu) group as a candidate for the acyl group of the LCST molecules.

The molar mass of LCST materials, an important factor limiting the maximum effective concentration of the molecules, was determined by the selection of backbone molecules with amine groups. Two draw solutes, *n*Bu-TAEA and *n*Bu-PEI (Fig. 1), were synthesized through an acylation reaction between the backbone molecules and *n*-butyric anhydride. As for *n*Bu-TAEA, all three primary amine groups were acylated to produce a molecule with a molar mass of 356 g/mol. For *n*Bu-PEI, about 87% of the reactable amine groups, primary and secondary amines of *b*-PEI, were reacted into *n*-butyramides to produce a polymer with an average molar mass (M_n) of 1,238 g/mol. The reaction was quite efficient,

and the yields were almost 100% in both cases. Aqueous solubility of both draw solutes was well over 70 wt% below the phase transition temperature. The molarities of the 70 wt% solutions were 2.1 M and 0.57 M for *n*Bu-TAEA and *n*Bu-PEI at 25 ℃, respectively. The physicochemical characteristics of both LCST molecules are summarized in Table 1.

In addition, although there is still a tertiary amine in an *n*Bu-TAEA molecule, the *n*Bu-TAEA solution (1.0 M) has a mild pH value of 7.7. The electron-withdrawing effect of the three amide groups and the hydrophobic steric factor can effectively lower the pK_a of *n*Bu-TAEA to about 5.9, which is significantly lower than other tertiary amines such as triethylamine (pK_a = 10.7).

3.2. Thermoresponsiveness of prepared molecules

3.2.1. *n*Bu-PEI and *n*Bu-TAEA

In most cases, the entropy of mixing LCST materials and water (ΔS_{mix}) is negative, and phase separation occurs at a temperature where the Gibbs free energy of mixing ($\Delta G_{mix} = \Delta H_{mix} - T\Delta S_{mix}$) becomes positive.[15] Thermoresponsive phase transition of LCST mixtures induces an abrupt increase of turbidity at the phase transition temperature, which can be easily measured by temperature-controlled UV/Vis spectrometry. The abrupt increase of turbidity or decrease of transmittance of *n*Bu-TAEA and *n*Bu-PEI mixtures is shown in Fig. 2. Although more precise method for

measuring phase transition temperature could be observation of light scattering, the turbidimetry is the most convenient and simplest method.[4] The phase transition temperature varied with the composition of the LCST mixtures, and the corresponding phase diagram is shown in Fig. 3. Because molarity is temperature dependent, I show the weight percentage-temperature phase diagrams of the LCST mixtures in Fig. 3. (The molarity-temperature phase diagrams are shown in Fig. 4, based on the molarity at 25 ℃). In wide composition ranges, both LCST mixtures showed phase transition temperatures around 30 ℃, which could be very promising for practical desalination because heat energy input to induce the phase separation for the decrease of effective concentrations should be minimized by mild temperature changes.

As shown in Fig. 5, the transparent LCST mixture below the phase transition temperature became turbid rapidly, and was soon phase-separated into upper water-rich and lower solute-rich phases.

3.2.2. Glycol ethers (GEs)

The GEs were expected to exhibit a LCST transition because the hydrophilic oligoglycol moieties and the hydrophobic alkyl groups were well-balanced in its molecular structure. Notably, modulation of the phase transition temperature is possible because various types of GEs can be synthesised using Williamson ether synthesis to display different oligoglycol and alkyl moieties.[16]

Phase diagrams of the aqueous mixtures with DEH, DPP, and

PB are shown in Figure 6. The DEH/water and DPP/water mixtures exhibited U-shaped phase diagrams with one-phase miscibility at low temperatures and two-phase separation at high temperatures (Fig. 6a and 6b). However, the PB/water mixture exhibited one-phase miscibility at both low and high concentrations of PB and two-phase separation in the middle at all temperatures between 0 ℃ and 100 ℃ (Fig. 6c). For DEH and DPP, the phase transition from one phase to two phases occurs at approximately 20 ℃ for a wide range of compositions. When the temperature of the GE solutions increases beyond the phase transition temperature, they become phase-separated into two liquid phases, a GE-rich phase and a water-rich phase. Molality-based phase diagrams of the GE/water mixtures are also shown in Figure 7.

3.2.3 Composition of GEs in water- and GE-rich phases

The composition of a one-phase GE/water mixture at low T is determined by the amount of dissolved GE. On the other hand, the composition of the water-rich phase and the GE-rich phase at high T can be predicted from the phase diagram, in which the points on the phase separation line indicate the compositions of the separated phases. The composition of each phase at 30, 40, and 50 ℃ was measured using ^{1}H-NMR and compared with the value predicted from the phase diagram (Table 2). The two methods produced similar results, particularly for the concentrations of the water-rich phase.

4. Conclusions

Low MW molecules with delicate balance of hydrophilicity and hydrophobicity showed LCST phase transition behavior. *n*Bu-TAEA and *n*Bu-PEI which were derived from pre-existing higher MW polymer showed LCST phase transition and higher water solubility. Increased hydrophobicity which contributes negative entropy of mixing compensated increased statistical entropy of mixing because of lowered MW. GEs with adequate hydrophilicity balance also showed LCST phenomena. Thus, it could be concluded that delicate balance of hydrophilicity and hydrophobicity can induce LCST characteristics although the MW of the molecules is not sufficiently high. The changed solubility driven by LCST resulted in corresponding change of effective concentration.

5. References

[1] F. Liu, M. W. Urban, *Prog. Polym. Sci*. 2010, 35, 3.

[2] Y. Lee, K. Kataoka, *Soft Matter* 2009, 5, 38.

[3] D. Pissuwan, S. M. Valenzuela, M. B. Cortie. *Trends Biotechnol.* 2006, 24, 62.

[4] H. G. Schild, *Prog Polym Sci* 1992, 17, 163.

[5] J. S. Scarpa, D. D. Mueller, I. M. Klotz, *J. Am. Chem. Soc*. 1967, 89, 6024.

[6] L. H. Gan, Y. Y. Gan, G. R. Deen, *Macromolecules* 2000, 33, 7893.

[7] J.-S. Park, Y. Akiyama, F. M. Winnik, K. Kataoka, *Macromolecules* 2004, 37, 6786.

[8] L. E. Bromberg, E. S. Ron, *Adv. Drug. Deliv. Rev*. 1998, 31, 197.

[9] A. P. Nowak, V. Breedveld, L. Pakstls, B. Ozbas, D. J. Pine, D. Pochan *et. al., Nature* 2002, 417, 424.

[10] B. Jeong, Y. H. Bae, S. W. Kim. *Macromolecules* 1999, 32, 7064.

[11] M. Hirose, O. H. Kwon, M. Yamato, A. Kikuchi, T. Okano, *Biomacromolecules* 2000, 1, 377.

[12] H. Wei, S.-X. Cheng, X.-Z. Zhang, R.-X. Zhuo, *Prog. Polym. Sci.* 2009, 34, 893.

[13] J. S. Scarpa, D. D. Mueller and I. M. Klotz*, J. Am. Chem. Soc*., 1967, 89, 1967.

[14] J.-S. Park, Y. Akiyama, F. M. Winnik and K. Kataoka, *Macromolecules*, 2004, 37, 6786.

[15] H. G. Schild, *Prog. Polym. Sci.*, 1992, 17, 163.

[16] A. Williamson, Philos. Mag., 1850, 37, 350; S. Paul and M. Gupta, *Tetrahedron Lett.,* 2004, 45, 8825.

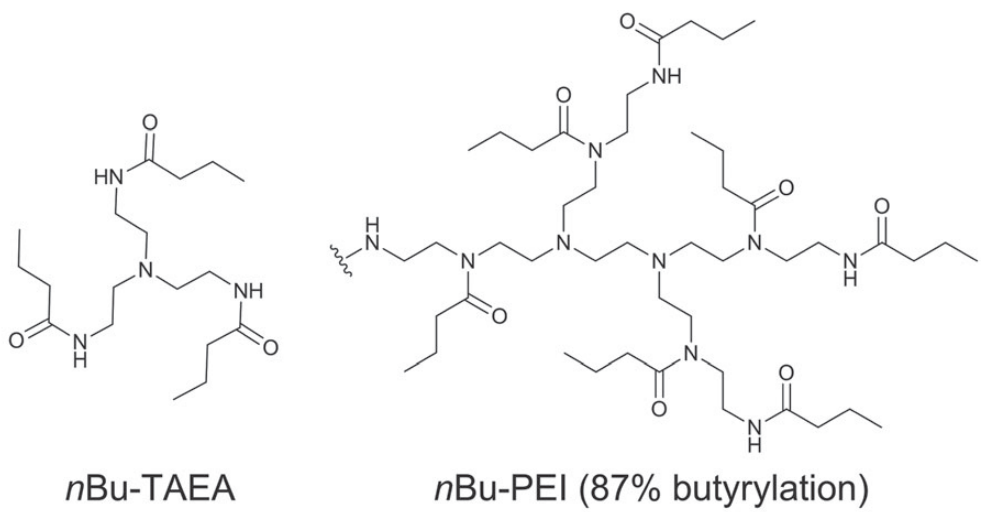

Figure 1. Structure of LCST materials synthesized by acylation

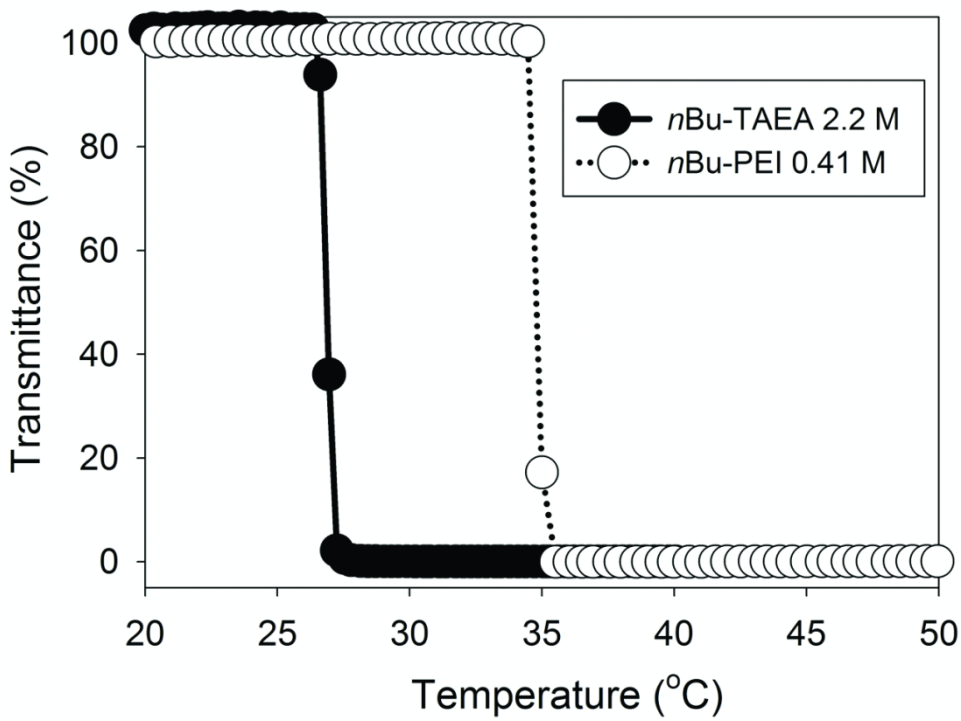

Figure 2. LCST phase transition of *n*Bu-TAEA and *n*Bu-PEI

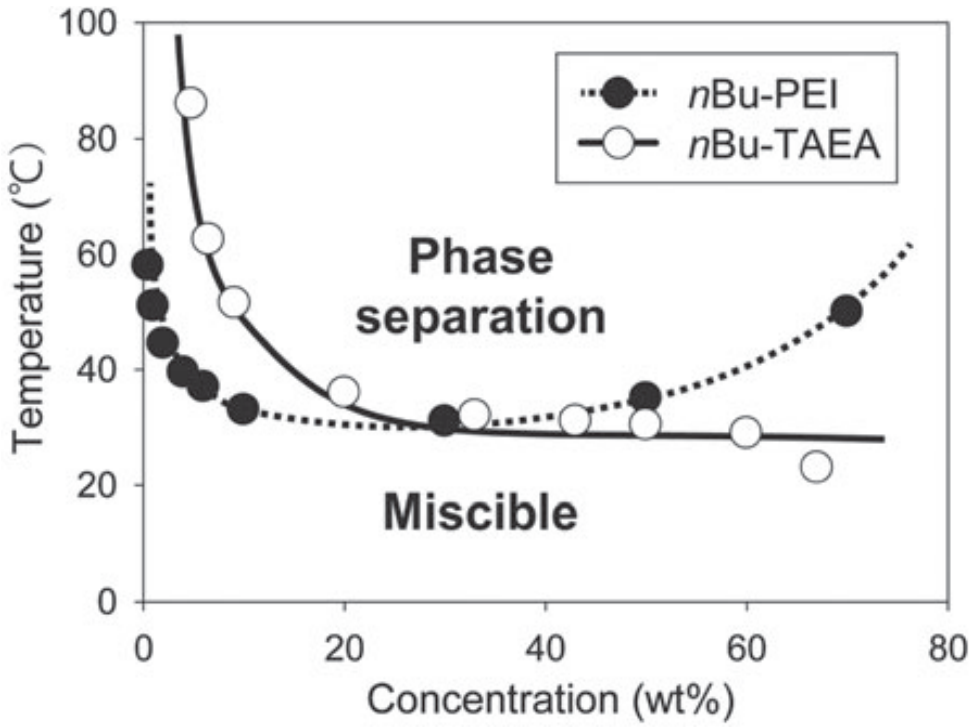

Figure 3. Phase diagram of the LCST material-water mixtures.

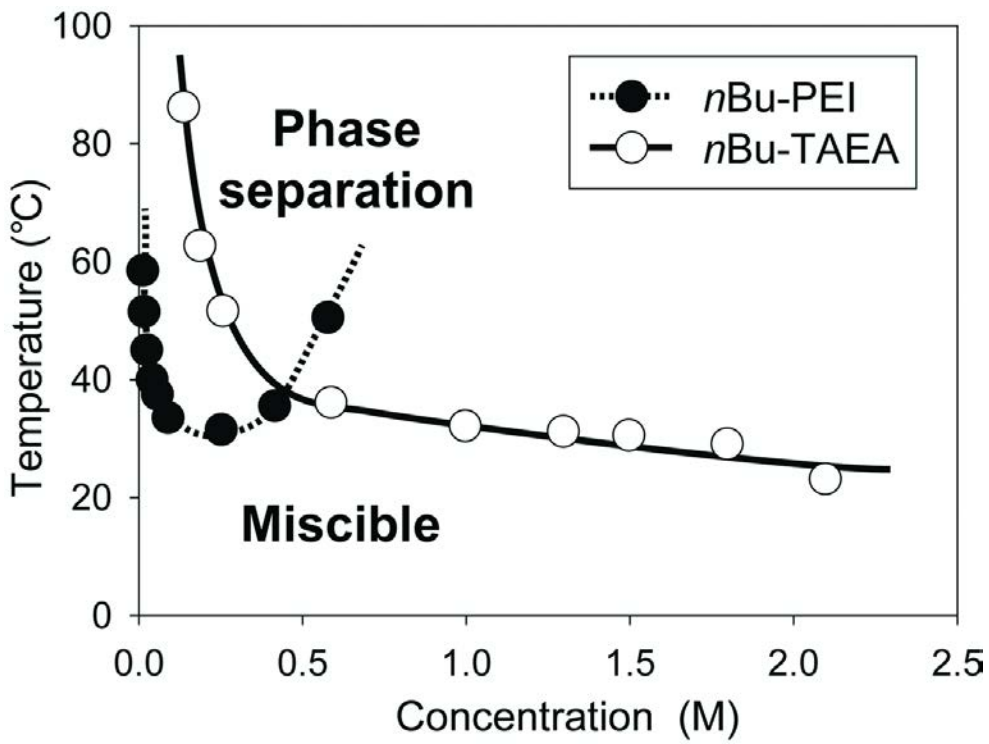

Figure 4. Molarity-temperature phase diagrams of *n*Bu-TAEA and *n*Bu-PEI

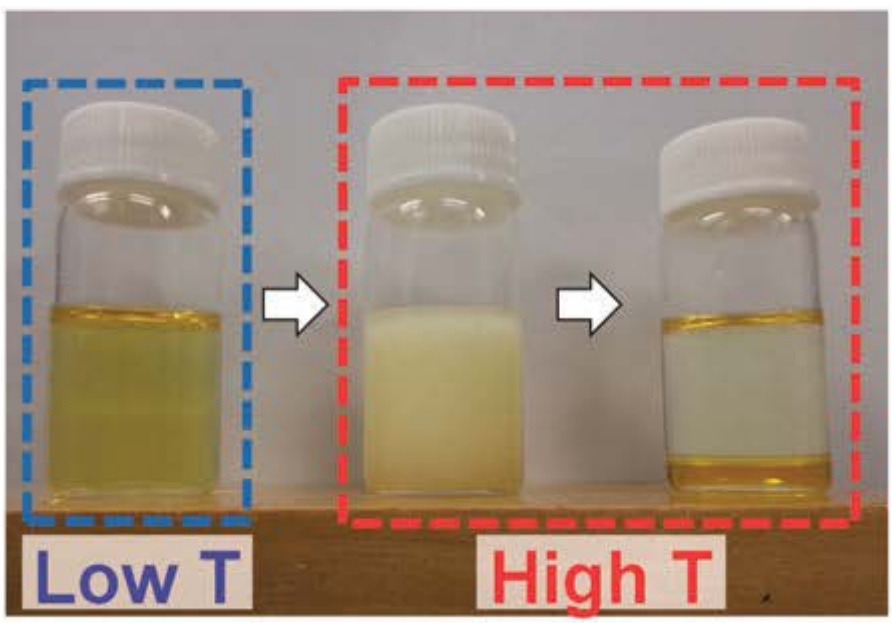

Figure 5. Temperature-dependent phase separation of an nBu-PEI-water mixture (composition: 11 wt%)

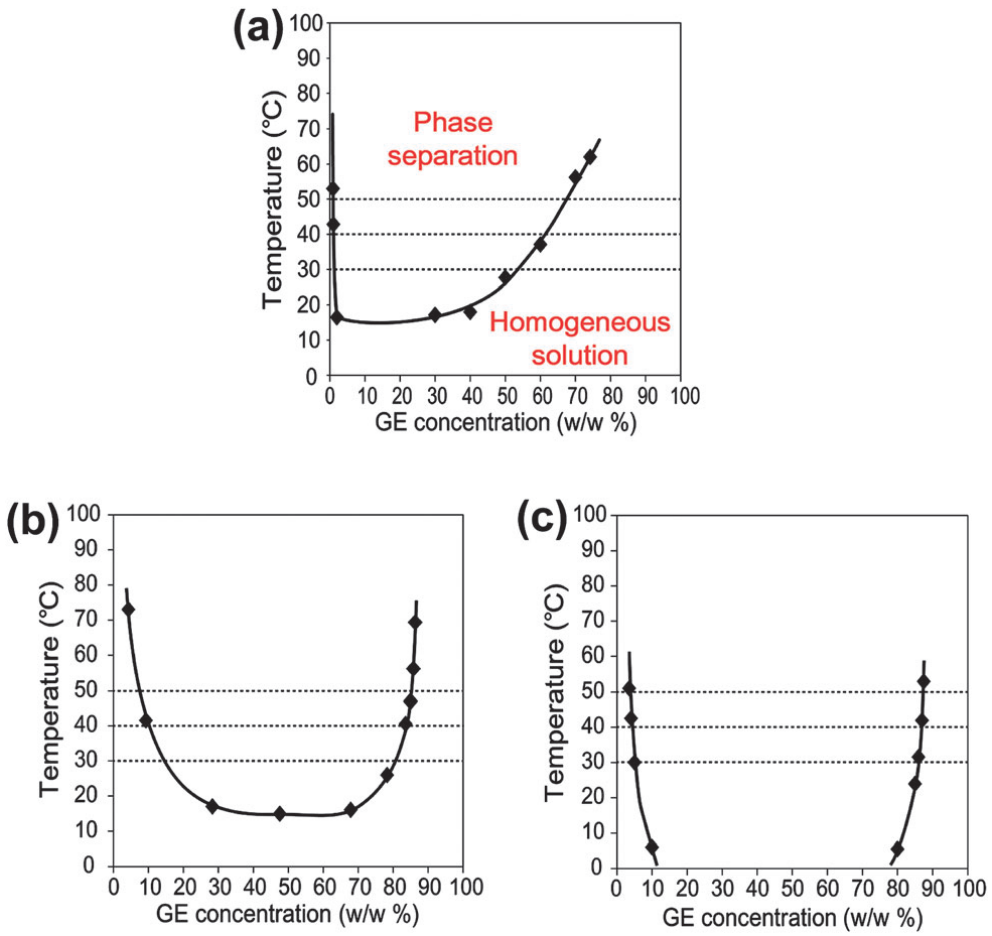

Figure 6. Phase diagrams of GE-water mixtures; (a) DEH-water, (b) DPP-water, and (c) PB-water.

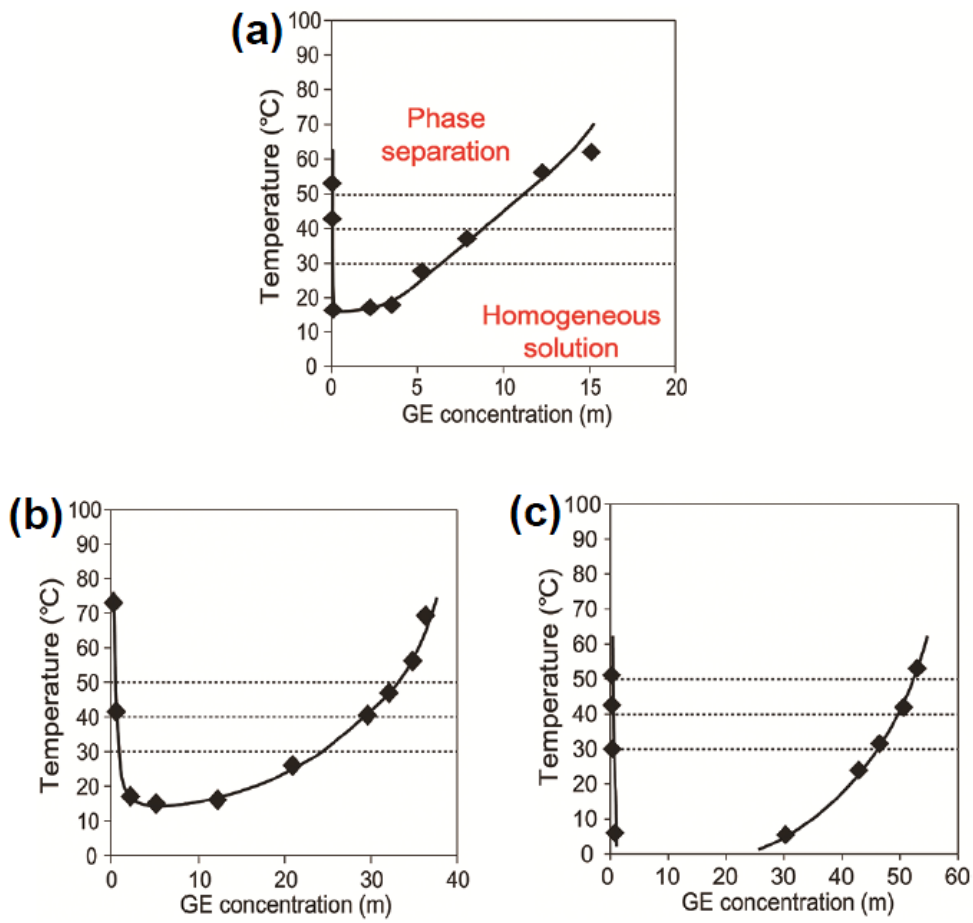

Figure 7. Molality-based phase diagrams of GE-water mixtures; a) DEH/water, (b) DPP/water, and (c) PB/water

Draw solutes	M (g mol^{-1})	Solubility (wt%)	Molarity[b] (mol L^{-1})	Phase transition temp. (°C)	Residual solute concentrations in the water-rich phase[c] (mol L^{-1})	Rejection efficiency[d] (%)
*n*Bu-TAEA	356	>80	>2.4	32 (1.0 M)	0.22	98.0
*n*Bu-PEI	1238[a]	>70	>0.57	31 (0.24 M)	0.052	99.6

[a] The molar mass of *n*Bu-PEI was derived from number-averaged molecular weight (M_n) determined by the ^{1}H-NMR spectrum. [b] The molarity was calculated on basis of the density at 25 °C. [c] After phase separation at 55 °C. [d] Rejection of solutes by the membrane. NaCl rejection efficiency was 98.4% under the same conditions.

Table 1. Physicochemical characteristics of *n*Bu−TAEA and *n*Bu−PEI.

Table 1 The GE concentration in each phase after the phase separation

		GE concentrations after phase separation (w/w%/m)					
		30 °C		40 °C		50 °C	
Draw solutes		PD[a]	NMR[b]	PD	NMR	PD	NMR
Water-rich phase	DEH	1.5/0.079	1.5/0.081	1.1/0.059	1.1/0.059	0.93/0.049	1.1/0.056
	DPP	16/1.1	13/0.82	9.9/0.63	8.3/0.51	7.3/0.45	7.5/0.46
	PB	5.0/0.40	4.7/0.37	3.9/0.30	3.7/0.29	3.6/0.28	3.4/0.27
GE-rich phase	DEH	53/5.8	70/12	62/8.4	75/16	67/11	79/19
	DPP	81/24	77/19	84/29	79/21	85/33	79/22
	PB	86/46	88/53	87/49	89/60	87/49	91/77

[a] Concentrations based on the phase diagram. [b] Concentrations measured by ^{1}H-NMR in GE–D_2O mixtures.

Table 2. The GE concentration in each phase after the phase separation.

Part II. Photoisomerization-Induced Modulation of Lower and Upper Critical Solution Temperature Phase Transition Behavior of Branched Polyethylenimine Derivatives in Water

1. Introduction

Stimuli-responsive materials responding to small changes in the environmental condition have raised great interests in the field of nano- and bioscience.[1-3] Such physicochemical stimuli include temperature change, light irradiation, pH, ultrasounds, reductive potential, *etc*. More sophisticated responsiveness can be achieved by combining one stimulus with another.[4,5] Combination of thermo- and light responsive properties, which have been predominantly focused features on smart materials,[6] was first reported 3 decades ago.[7] Menzel and coworkers[8] affirmed that statistical copolymers originated from *N,N*-dimethylacrylamide and 4-phynylazophenyl acrylate show shift of lower critical solution temperature (LCST) phase transition points upon UV-light irradiation up to 20 ℃ in water. After this work there have been intensive researches to study and develop the dual-responsive polymers[9-12] and they have been realized in various applications.[13-15] However, the swing of phase transition temperature upon irradiation has been limited under several degrees Celsius,[9-12] which still has not overcome the shift of Menzel *et al.*[8]

Photo-control of upper critical solution temperature (UCST) phase behavior has also been investigated in recent five years.[16-18] Unlike LCST in which polymer solutes mix in cold solvent and separates from the solvent upon phase transition temperature, homogeneous solution of UCST polymers show phase separation

below certain temperature because of positive enthalpy of mixing ($\Delta H_m > 0$) originated from strong solute−solute interactions predominating over those of solute−solvent.[19] The first example of UCST photo−control to the best of my knowledge is copolymers comprising *N*−isopropylacrylamide and 4−phenylazophenyl methacrylate reported by Watanabe *et al.*[16] The copolymers show UCST transition in ionic liquids and the phase transition points can be decreased by 43 °C after irradiation of UV−light. Although there have been a few studies demonstrating photo−tunable UCST property in alcohol[17] and ethanol−water mixture,[18] still this feature has not been realized in polymer−water binary systems.

I have studied thermoresponsive properties of branched polyethylenimine (*b*−PEI) derivatives in aqueous solution. Water−soluble *b*−PEIs have high amine density (one per 43 g mol^{-1}) capable of substitution with certain electrophiles. Acylation of *b*−PEI with acyl anhydrides yields LCST properties by increased hydrophobicity resulting in negative entropy of mixing ($\Delta S_m < 0$).[20] *b*−PEI attached with sulfopropyl group after reaction with 1,3−propanesultone shows UCST properties induced by increased electrostatic interaction between zwitterionic polymer residues, causing positive ΔH_m.[21] Thus, I hypothesized that implantation of L/UCST−inducing groups and light−responsive chromophore in *b*−PEI may lead photo−tunable thermoresponsive properties (Fig. 1).

In this part I present two types of L/UCST polymers responding to light irradiation in aqueous system; acylated *b*−PEI containing azobenzene (Ab) moiety (Ab−Pr−PEI) with LCST shift up to

33.1 ℃ after irradiation and Ab-containing propanesulfonated *b*-PEI (Ab-PS-PEI) demonstrating for the first time light-induced alternation of UCST.

2. Experimental Details

2.1. Synthesis of light-tunable LCST polymers

Azobenzene (Ab)-containing propionylated *b*-PEI (Ab-Pr-PEI) was synthesized as below. 1.20 g *b*-PEI (27.9 mmol amine residues) and 4 mL of TEA (28.7 mmol) were dissolved in 30 mL of DCM and then chilled on ice. 1mL of DCM solution dissolving 306.7 mg 4-phenylazobenzoyl chloride (1.25 mmol; 0.0600 eq. to reactive amine residues and 0.0450 eq. to total amine residues) and 0.913 mL propionyl chloride (10.5 mmol; 0.375 eq. to total amine residues) was added dropwise to the solution. After 30 minute the reaction temperature was adjusted to room temperature and proceeded overnight. The Ab-Pr-PEI in the reaction mixture was purified by dialysis. Using dialysis membrane with molecular-weight-cut-off (MWCO) 6000 Da the reaction mixture was dialyzed with methanol 2 times and deionized water 5 times. The solution in the dialysis bag was stirred an hour in 0 ° C and centrifuged in 2 ° C to obtain water-soluble part from reaction products. The supernatant was freeze-dried, yielding 3 mol% (to the total amine residues) Ab and 34 mol% propionyl groups-substituted polymer; Ab_3-Pr_{34}-PEI. The degrees of substitution were calculated based on integration ratios in ^{1}H-NMR spectra (Fig. 2). The light and thermoresponse can be varied by different degree of substitution. Ab-Pr-PEI with different Ab feed ratio (0.0225 eq. to total amine residues) was also obtained. The reaction feed and final substitution degrees are summarized in Table 1.

2.2. Synthesis of light-tunable UCST polymers

Ab-containing propanesulfonated *b*-PEI (Ab-PS-PEI) was synthesized as below. 1.5 g *b*-PEI (34.8 mmol amine residues) was dissolved in 30 mL of DCM and then chilled on ice. 255.6 mg 4-phenylazobenzoyl chloride (1.04 mmol; 0.0300 eq. to total amine residues) was dissolved in 1 mL of DCM and then added dropwise to the *b*-PEI solution. After 20 minute the reaction mixture was stirred 2 hours at room temperature. 0.764 mL of 1,3-propanesultone (8.71 mmol; 0.250 eq. to total amine residues) and 30 mL of methanol were added to the reaction mixture then the reaction temperature was adjusted to 45 ℃. The reaction proceeded overnight. RBF containing the reaction mixture was not perfectly closed to avoid probable explosion by boiled DCM vapour. Then 20 mL of 3N NaOH was added to the reaction mixture and the mixture was sonicated 10 minute at 50 ℃. After dialysis (3 times at the room temperature and 4 times at 40 ℃) using 6000 Da MWCO membrane, the solution in the dialysis bag was stirred an hour at 80-90 ℃. The solution was filtered to obtain water-soluble part and the filtrate was freeze-dried. Degrees of substitution were 0.8 and 24 mol% for Ab and propanesulfonyl group ($Ab_{0.8}$-PS_{24}-PEI), respectively, calculated by ^{1}H-NMR spectra (Fig. 3). Two different Ab-PS-PEIs having varied feed ratio were synthesized with same method (Table 1).

2.3. Characterization of thermoresponsive behavior

The LCST or UCST type phase transition temperature was measured by turbidimetry at 600 nm light using UV-visible spectrometer (Jasco V-650, Japan). For LCST measurement, transmittance of clear aqueous solution at low temperature was adjusted as 100% and the solution was heated with ramping rate of 1 ℃/min. After the phase transition condition the transmittance decreased below 1%. The temperature at 50% transmittance was defined as the phase transition temperature, also called as a cloud point. UCST phase transition temperature was also defined using same method above but cooling clear solution at high temperature to low temperature.

2.4. Photochromism of Ab-Pr-PEI and Ab-PS-PEI

Light-responsive *trans*-to-*cis* isomerization was determined by change in absorption spectra of sample solutions (Fig. 4). Irradiation was carried out using 100W high-pressure mercury lamp (Lichtzen, South Korea) equipped with fiber optics and band-pass filters (Edmund optics, US). For UV irradiation, a 357 nm band-pass filter with 48 nm full width-half-max (FWHM) was used (OD > 6.0). For visible irradiation, a 440 nm band-pass filter with 46 nm FWHM was used (OD > 6.0). Light intensities were 8 mW/cm^2 and 5 mW/cm^2 for UV and visible irradiation, respectively.

2.5. Reversibility of light-tuned phase transition

Cloud points at repeated UV and visible irradiation were measured. In case of Ab_3-Pr_{34}-PEI, phase transition temperature of 0.3 wt% solution stored in the dark was first measured. 3 cycles of UV and visible irradiation was then performed. One cycle comprised 'UV part' and 'visible part'. In an 'UV part' sample was irradiated upon UV light for 30 minute at low temperature (below 20 ℃). A 'visible part' includes visible irradiation for 30 minute at same low temperature and then storing the sample at 70 ℃ for an hour in the dark. In case of 0.3 wt% $Ab_{0.8}$-PS_{24}-PEI solution, the UCST sample, phase transition temperature of 0.3 wt% solution stored in the dark was first measured. 3 cycles of UV and visible irradiation was then performed with the method of Ab_3-Pr_{34}-PEI but storing time at 70 ℃ in visible part was 30 minute. Use of intensive light (> 30 mW/cm^2) without cooling (< 20 ℃) yielded irreproducible change in the phase transition temperature probably caused by irreversible photoreaction of Ab moieties.

2.6. Light-induced isothermal phase transition

Reversible phase transition caused by UV or visible irradiation was measured at fixed temperature in between cloud points without irradiation and with UV irradiation. Aqueous solution of 0.3 wt% Ab_3-Pr_{34}-PEI was first UV-irradiated for 1 hour at low temperature below 20 ℃ and then the temperature was elevated to 36 ℃. Visible light from fiber optics of the mercury lamp was irradiated perpendicularly to the cuvette containing the UV-

irradiated solution during 4000 seconds. UV irradiation was followed after the 4000 seconds visible irradiation. The transmittance at 700 nm before visible irradiation was adjusted as 100 % and change in the transmittance was recorded as a function of time upon sequential visible and UV irradiation described above. 0.3 wt% $Ab_{0.8}$–PS_{24}–PEI solution was also examined in the same manner, but with different temperature at 13.5 ℃.

3. Results and Discussion

3.1. Synthesis of light-responsive L/UCST polymers

Light- and thermoresponsive *b*-PEI derivatives were prepared by nucleophilic substitution. As an LCST-type model, *b*-PEI (M_n = 10 000, PD(M_w/M_n) = 2.5) was reacted with 4-phenylazobenzoyl chloride and propionyl chloride. ^{1}H-NMR spectra (Fig. 2) revealed the degrees of substitution in initial total amine residues were 3 mol% and 34 mol% for azobenzoyl- and propionyl group, respectively (Ab_3-Pr_{34}-PEI). An UCST-type model was obtained by reaction of same *b*-PEI with 4-phenylazobenzoyl chloride and 1,3-propanesultone, resulting in 0.8 mol% and 24 mol% substitution of azobenzoyl- and propanesulfonyl group, respectively ($Ab_{0.8}$-PS_{24}-PEI; Fig. 3). Detailed synthetic information is summarized in Table 1. The synthetic protocol to obtain light- and thermoresponsive polymers in this study is similar with the strategy of Jochum *et al.*[22] They synthesized dual-responsive copolymers *via* polymer analogous reaction in which pre-synthesized polymeric precursor reacts with various functional amines. Unlike conventional methods copolymerizing Ab containing monomers and LCST-inducing monomers such as *N*-isopropylacrylamide, the presented post-modification approaches may give products constant degree of polymerization and structural versatility.

3.2. Thermoresponsiveness of PEI derivatives

Aqueous solutions of the synthesized *b*-PEI derivatives stored in the dark exhibited either LCST or UCST type phase transition (Fig. 5-9). The LCST phase transition temperature of Ab_3-Pr_{34}-PEI decreased as the concentration increased following typical LCST phase diagram with shape of convex downward in the measurement range (Fig. 5a).[23] Considering the phase transition temperature of propylated *b*-PEI with similar substitution degree was shown within 50-60 ℃, Ab moieties may have lead decrease of phase transition temperature caused by increased hydrophobicity.[20] This tendency was agreed comparing Ab_3-Pr_{34}-PEI with similar *b*-PEI derivative which has less amount of Ab substitution (Ab_2-Pr_{32}-PEI; Fig. 6). The cloud point of 0.5 wt% Ab_3-Pr_{34}-PEI solution was 19.9 ℃ which was smaller than that of 0.5 wt% Ab_2-Pr_{32}-PEI with 14.5 ℃ difference.

The UCST-type phase transition properties of $Ab_{0.8}$-PS_{24}-PEI were opposite with LCST-type samples. The UCST phase transition temperature of $Ab_{0.8}$-PS_{24}-PEI solutions increased with increase of concentration following upward convex shape of UCST phase diagram (Fig. 5b).[19] 0.5 wt% $Ab_{0.8}$-PS_{24}-PEI solution showed phase transition at 23.4 ℃ and less Ab-substituted $Ab_{0.5}$-PS_{22}-PEI in same concentration phase-separated at 19.9 ℃ (Fig. 7). Increased hydrophobic interaction by higher composition of Ab moiety would contribute stronger solute-solute interaction as well as increase in ΔH_m, resulting in increase of phase transition temperature.[24]

3.3. Photochromism of PEI derivatives

Reversible *trans*−*cis* Ab isomerization by UV and visible light irradiation was confirmed by observing change of absorption spectra (Fig. 4) In case of Ab_3−Pr_{34}−PEI, an LCST−type model, decrease of absorption band at 327 nm (π–π*) and increase at 430 nm (n–π*) upon UV irradiation were observed, where full recovery was obtained after visible irradiation and heating. Similar spectral change was observed for UCST−type $Ab_{0.8}$−PS_{24}−PEI at 331nm (π–π*), whereas n −π* transition was shown as a shoulder peak at a shorter wavelength. ^{1}H−NMR study also agreed the increasing amount of *cis*−Ab moiety up to 66 mol% at the photo stationary states upon UV irradiation and recovery of *trans*−dominant states after visible light irradiation and heating (Fig. 10).

3.4. Shifts of L/UCST upon UV irradiation

Upon UV irradiation, both L/UCST−type phase transition temperatures were changed from the original ones (Fig. 8). Ab moiety shows reversible *trans*−*cis* isomerization accompanied by the alteration of dipole moment from 0 Debye for *trans* isomer to 3 Debye for *cis* isomer.[25] The increased polarity of the polymer solution after UV irradiation would result in shift of phase transition behavior. For LCST models, decreased hydrophobicity by *cis*−rich photo stationary states resulted in increase of transition points (Fig. 8a). The phase transition temperature of 0.5 wt% Ab_3−Pr_{34}−PEI solution after UV irradiation recorded 53.0 ℃ which was 33.1 ℃

increased from that of the dark solution. Generally, the UV-induced shift of phase transition temperatures have been found within a few degrees Celsius[7,9-13,22], with one exception of 20 ℃ difference.[8]

The reason of the unusual large transition shift observed in the present case seems difficult to be clarified. One reason could be described comparing the contribution of Ab moieties to overall hydrophilic and hydrophobic balance in the polymer. The majority of reported dual responsive polymers have comprised 3 parts of hydrophobic regions; polymer backbones, Ab moieties and alkyl groups, causing the formation of water cage with entropic loss for mixing.[26] However, in case of Ab-substituted acylated PEIs the hydrophobicity of polymer backbone would be much smaller than that of conventional polymers since the PEI derivatives contain repeating nitrogen atoms (one per two carbons) in their backbone unlike hydrophobic hydrocarbons in the conventional polymer backbone. This feature may lead weaker formation of water cage in the backbone; hence the hydrophobic characteristics making negative □S_m would be comprised mainly by two; Ab and propionyl groups in the PEI derivatives. Therefore, the influence of Ab moieties to the total hydrophobicity balance will be increased, resulting in remarkably larger shift of phase transition points.

In case of $Ab_{0.8}$-PS_{24}-PEI, UCST phase transition points of 1 wt% solution decreased from 42.0 ℃ to 36.4 ℃ after UV irradiation. (Fig. 8b) Decrease in positive ΔH_m by weakened hydrophobic interactions between Ab moieties with higher *cis* content produced

upon UV irradiation may result phase transition at lower temperature. Lower amount of UCST shift compared with LCST-type Ab_3-Pr_{34}-PEI probably seems because of smaller Ab substitution (0.8 mol% to total PEI amine residues). Increased UCST shift was observed in 1 wt% Ab_3-PS_{43}-PEI solution from 57.4 ℃ to 35.5 ℃ after UV irradiation (Fig. 9). Recent studies have revealed that Ab-modified UCST polymers containing oligo ethylene glycol[17], isopropyl amide or hydroxyl groups[18] show UCST properties in alcohol, but not in water. These groups may not be sufficient to obtain stronger solute-solute interaction overcoming interaction of solute-water molecules. Introduction of zwitterionic groups, *e.g.* propanesulfonylation into *b*-PEI yielding sulfopropyl ammonium moiety could result in UCST property in water by strong electrostatic solute-solute interaction.[21] To the best of my knowledge, this is the first demonstration of photo-induced UCST shift in 100 % water solution.

3.5. Reproducibility of L/UCST shifts

Furthermore, reversible L/UCST shifts were observed upon sequential UV and visible irradiation (Fig. 11 and Fig. 12). As expected from the changes in absorption spectra of L/UCST solutions upon UV and visible irradiation (Fig. 4), visible light recovered the phase transition temperature which was shifted upon UV-irradiation. Decrease in phase transition temperature was observed at visible light irradiation to the UV-irradiated Ab_3-Pr_{34}-PEI solution (0.3 wt%; Fig. 11). Difference between the phase

transition temperature under dark and visible light conditions seemed because of higher content of *cis*–Ab in the photo–stationary state at a visible irradiation state rather than a dark. Meanwhile, the opposite tendency of the phase transition temperature shift was observed for $Ab_{0.8}$–PS_{24}–PEI solution (0.3 wt%) upon similar sequential irradiation (Fig. 12). These L/UCST shifts and recoveries were maintained over repeated 3 cycles of UV/Vis irradiation, indicating reproducibility of photo–modulated L/UCST shifts.

3.6. Photo–induced phase separation

To demonstrate photo–induced phase separation, transmittance of L/UCST solution upon irradiation at a fixed temperature was examined (Fig. 13 and Fig. 14). 0.3 wt% Ab_3–Pr_{34}–PEI solution was first irradiated under UV light for an hour, and change of transmittance was recorded upon sequential visible and UV irradiation at 36 ℃ (Fig. 13). This temperature is in between phase transition temperatures of *cis*–Ab rich and *trans*–Ab rich solutions at which the solution is bistable. Under visible irradiation, the solution became opaque with decreasing transmittance to 11% from 100% of the original solution. Changing light source to UV recovered the transmittance to its original higher values. Similar clouding and clearing was observed for 0.3 wt% $Ab_{0.8}$–PS_{24}–PEI solution at same experimental condition but transmittance decreased down to 38% upon visible irradiation (Fig. 14). For both L/UCST samples the clearing processes under UV light were

relatively slower than clouding processes under visible light.

4. Conclusions

Photo-control of LCST with greater shifts than previous reports and first photo-controlled UCST shifts in water were achieved in this study. Photo- and thermoresponse could be varied by concentration, degree of substitution, type of substituents, and irradiation with a facile one-step synthetic method maintaining degree of polymerization with all commercially available reagents without requiring monomer synthesis and polymerization steps. Relatively higher PD(M_n/M_w) value would be reduced using polymer precursor with low PD value such as linear PEI. Higher shifts of cloud points were understood regarding contribution of Ab moieties to total polymer hydrophobicity. (Fig. 15) Since synthesized polymers still possess reactive amine residues, post-conjugation with functional molecules such as enzymes and cell-penetrating peptides would be easily carried out. Moreover, since thermo-response of PEI derivatives are known to be sensitive to pH and additional salts, my L/UCST polymers would be quadruple-stimuli responsive, *i.e.*, to temperature, light, pH and ionic strength. Therefore, performance-controllable simple synthetic platform proposed in this study is expected to be applied to various fields such as hydrogels, drug delivery and water purification.

5. References

[1] M. A. C. Stuart, W. T. S. Huck, J. Genzer, M. Müller, C. Ober, M. Stamm, G. B. Suhorukov, I. Szleifer, V. V. Tsukruk, M. Urban, F. Winnik, S. Zauscher, I. Luzinov and S. Minko, *Nat. Mater.*, 2010, 9, 101.

[2] M. Molina, M. A.-Birjand, J. Balach, J. Bergueiro, E. Miceliac and M. Calderón, *Chem. Soc. Rev.*, 2015, 44, 6161.

[3] L. D. Zarzar, V. Sresht, E. M. Sletten, J. A. Kalow, D. Blankschtein and T. M. Swager, *Nature*, 2015, 518, 520.

[4] J. Zhuang, M. R. Gordon, J. Ventura, L. Li and S. Thayumanavan, *Chem. Soc. Rev.*, 2013, 42, 7421.

[5] P. Schattling, F. D. Jochum and P. Theato, *Polym. Chem.*, 2014, 5, 25.

[6] F. D. Jochum and P. Theato, *Chem. Soc. Rev.*, 2013, 42, 7468.

[7] D. Kungwatchakun and M. Irie, *Makromol. Chem., Rapid Commun.*, 1988, 9, 243.

[8] R. Kröger, H. Menzel and M. L. Hallensleben, *Macromol. Chem. Phys.*, 1994, 195, 2291.

[9] K. Sugiyama and K. Sono, *J. Appl. Polym. Sci.*, 2001, 81, 3056.

[10] A. Desponds and R. Freitag, *Langmuir*, 2003, 19, 6261.

[11] H.-i. Lee, J. Pietrasik and K. Matyjaszewski, *Macromolecules*, 2006, 39, 3914.

[12] X. Xue, J. Yang, W. Huang, H. Yang, B. Jiang, , F. Li and Y. Jiang, *Polymer*, 2015, 73, 195.

[13] T. Shimoboji, E. Larenas, T. Fowler, A. S. Hoffman and P. S. Stayton, *Proc. Natl. Acad. Sci. U. S. A.*, 2002, 99, 16592.

[14] Q. M. Zhang, W. Xu, and M. J. Serpe, *Angew. Chem. Int. Ed.*, 2014, 53, 4827.

[15] Z. Cao, H. Wu, J. Dong, and G. Wang, *Macromolecules*, 2014, 47, 8777.

[16] T. Ueki, Y. Nakamura, A. Yamaguchi, K. Niitsuma, T. P. Lodge and M. Watanabe, *Macromolecules*, 2011, 44, 6908.

[17] S. Wiktorowicz, H. Tenhu and V. Aseyev, *Macromolecules*, 2013, 46, 6209.

[18] Q. Zhang, P. Schattling, P. Theato and R. Hoogenboom, *Eur. Polym. J.*, 2015, 62, 435.

[19] J. Seuring and S. Agarwal, *Macromol. Rapid Commun.*, 2012, 33, 1898.

[20] H. Kim, S. Lee, M. Noh, S. H. Lee, Y. Mok, G.-w. Jin, J.-H. Seo and Y. Lee, *Polymer*, 2011, 52, 1367.

[21] M. Noh, Y. Mok, D. Nakayama, S. Jang, S. Lee, T. Kim and Y. Lee, *Polymer*, 2013, 54, 5338.

[22] F. D. Jochum and P. Theato, *Polymer*, 2009, 50, 3079.

[23] G. t. Brinket and F. E. Karasz, *Macromolecules*, 1984, 17, 815.

[24] M. Noh, S. Kang, Y. Mok, S. J. Choi, J. Park, J. Kingma, J.-H. Seo and Y. Lee, *Chem. Commun.*, 2016, 52, 509.

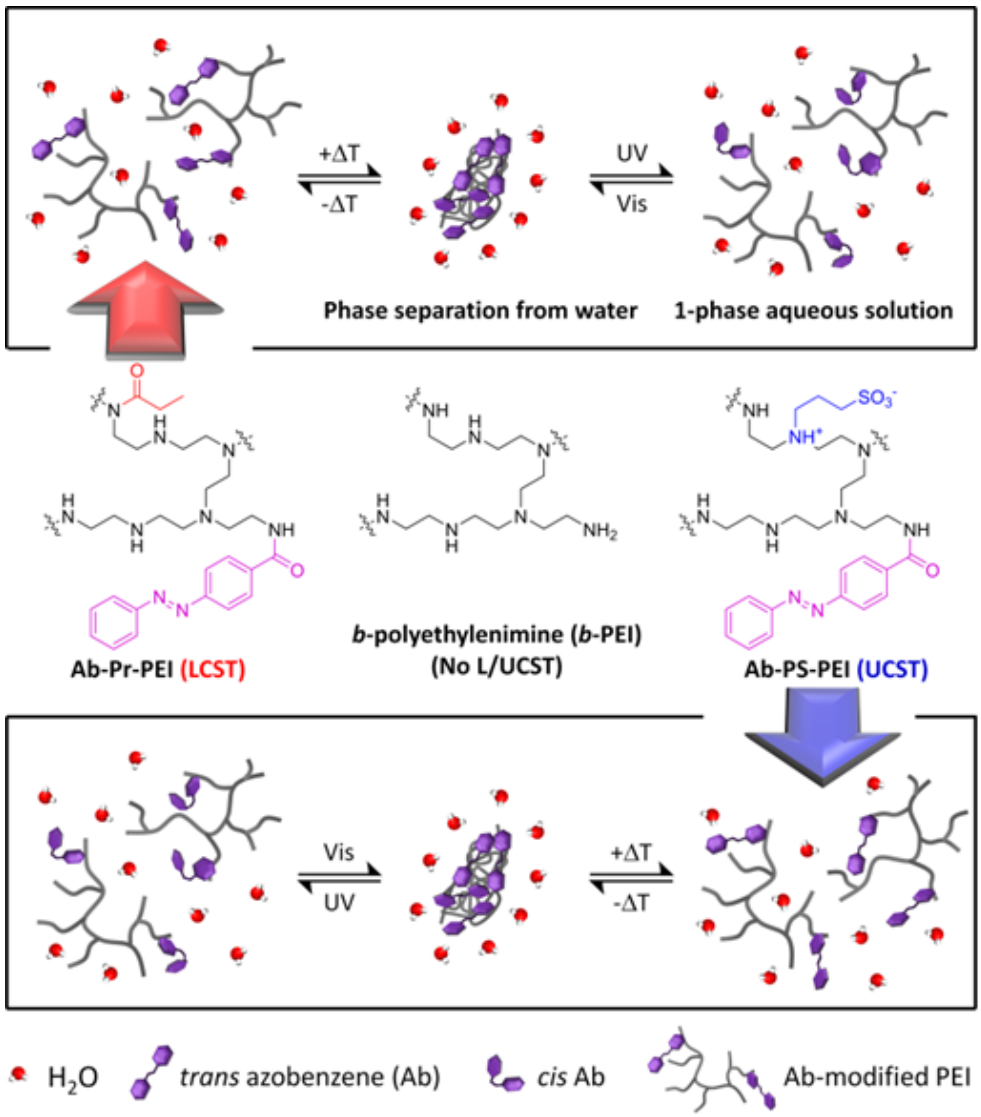

Figure 1. Chemical structures of *b*-PEI derivatives and schematic illustration of light-tuneable L/UCST-type phase transition

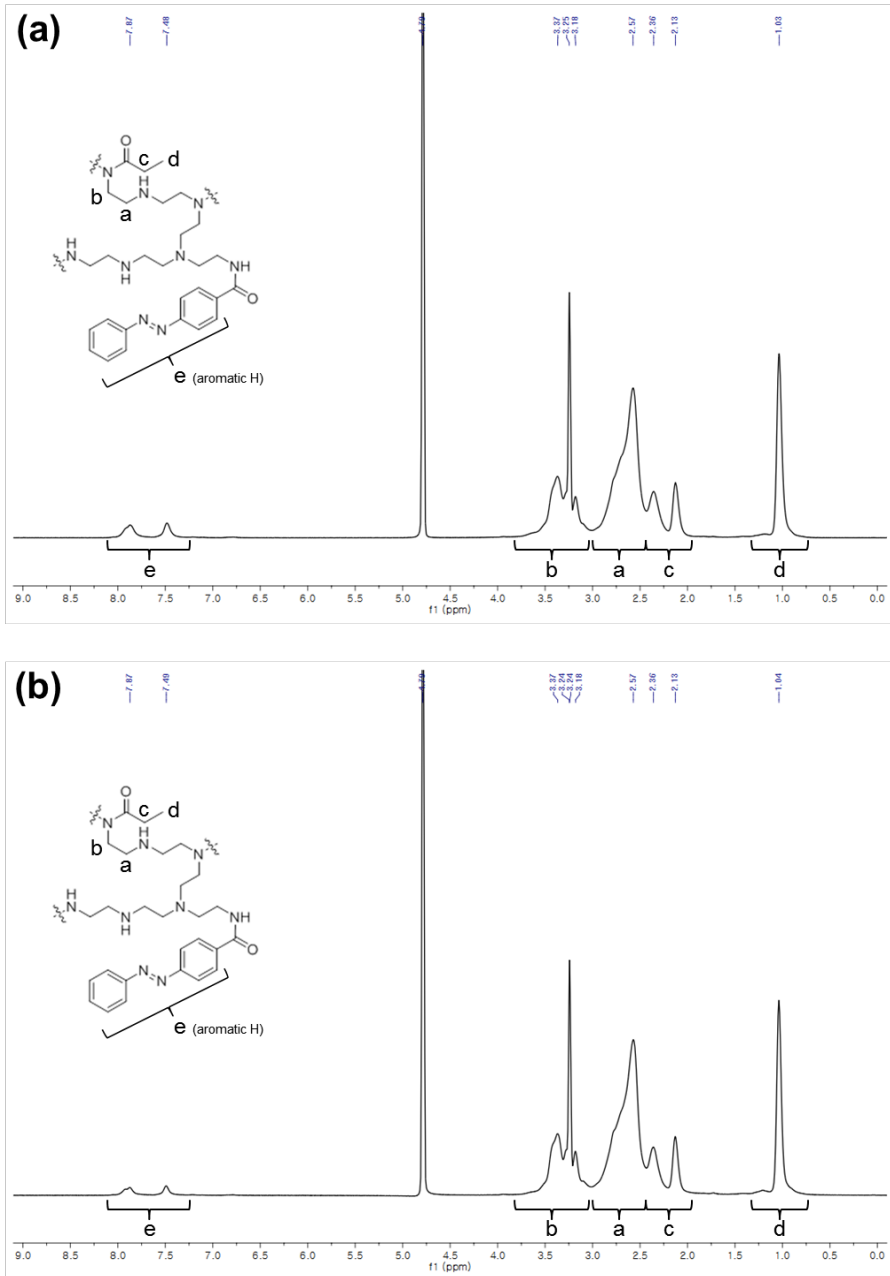

Figure 2. 1H-NMR spectra of (a) Ab_3-Pr_{34}-PEI and (b) Ab_2-Pr_{32}-PEI in CD3OD

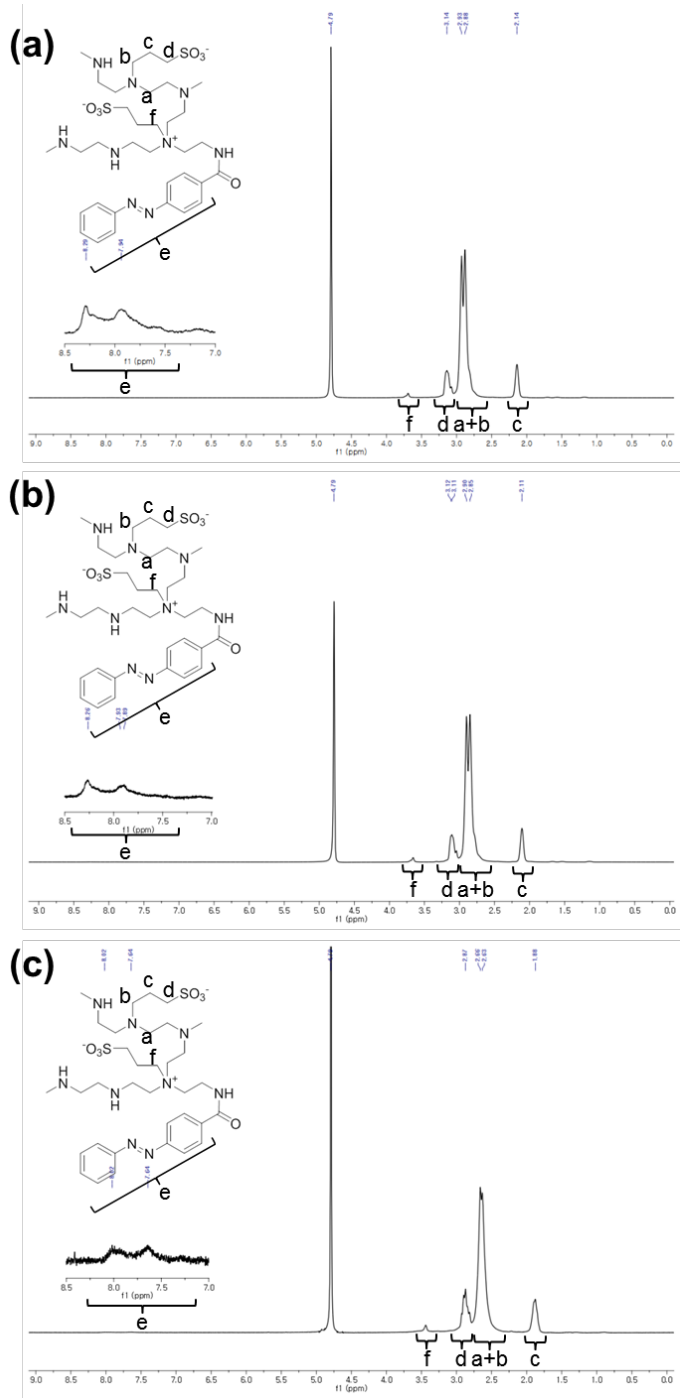

Figure 3. ^{1}H-NMR spectra of (a) $Ab_{0.8}-PS_{24}-PEI$, (b) $Ab_{0.5}-PS_{22}-PEI$ and (c) $Ab_{3}-PS_{43}-PEI$ in CD_3OD (1wt% NaOD).

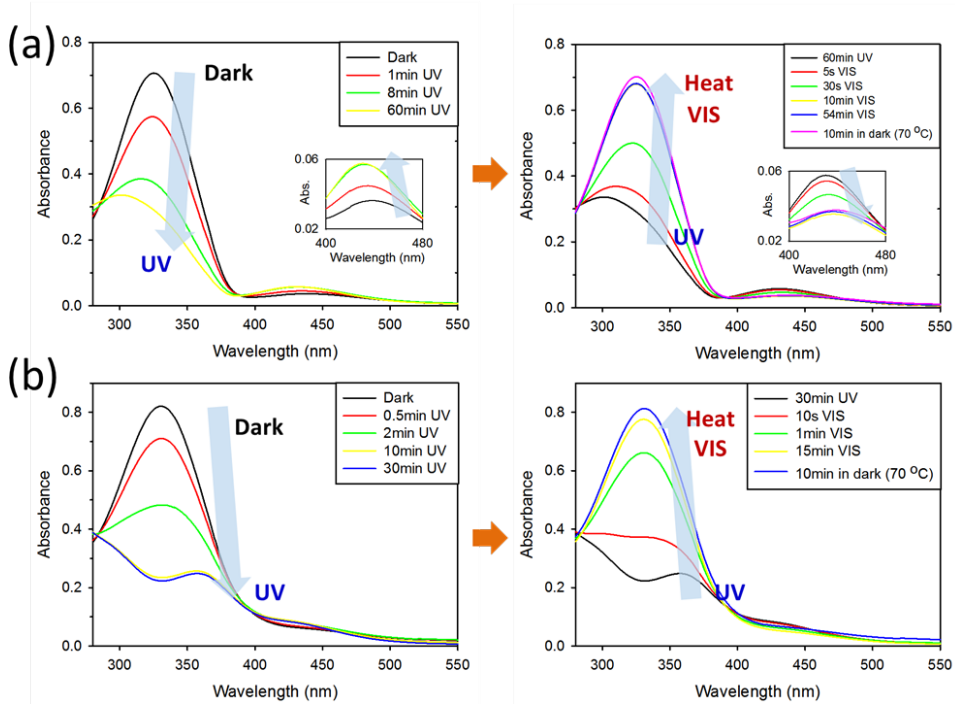

Figure 4. Absorption spectra of (a) 0.01 wt% Ab_3–Pr_{34}–PEI and (b) 0.3 wt% $Ab_{0.8}$–PS_{24}–PEI aqueous solution upon irradiation or heating at 15 and 35 ℃, respectively. UV–irradiated solutions (left) were irradiated by visible light and then heated (right). Absorbance of the sample solution at λ_{max} in UV region was decreased upon UV irradiation and nearly recovered to initial state upon the following visible light irradiation. Perfect recovery of the spectra was achieved after heating

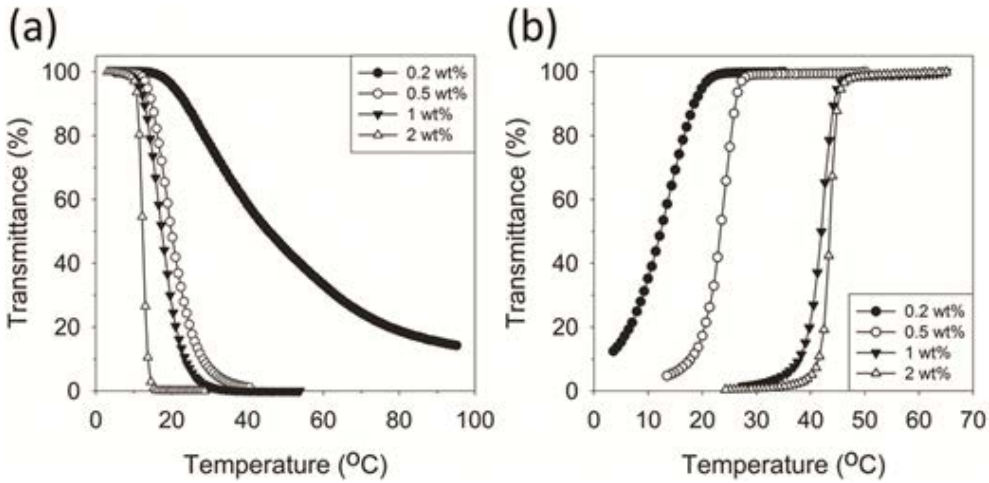

Figure 5. Phase transition of (a) LCST-type Ab_3-Pr_{34}-PEI and (b) UCST-type $Ab_{0.8}$-PS_{24}-PEI in water at various concentrations. Transmittance decreases at the phase transition temperature upon heating (a) or cooling (b).

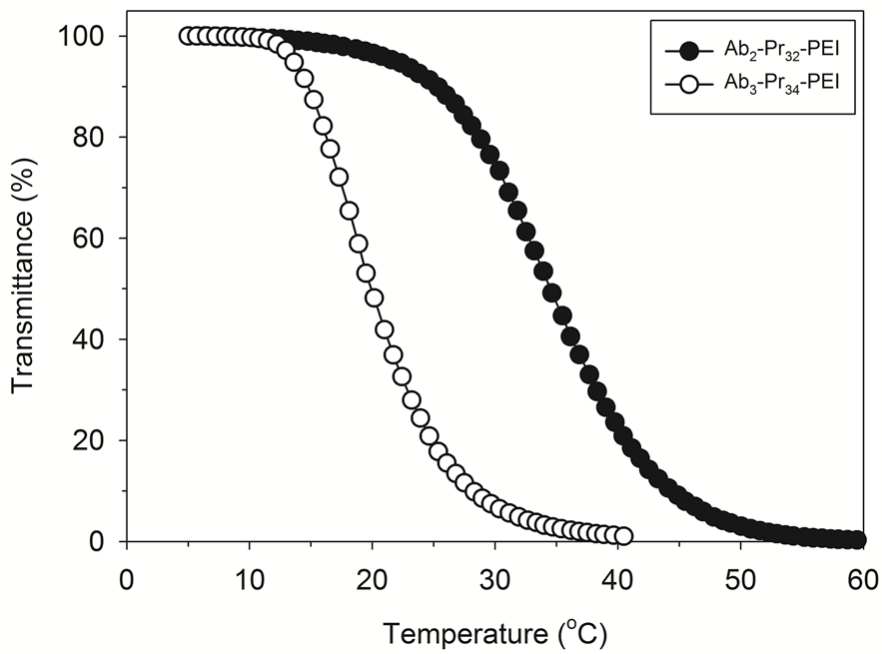

Figure 6. Influence of the Ab substitution degree on the LCST-type phase transition behaviour. (0.5 wt% in water)

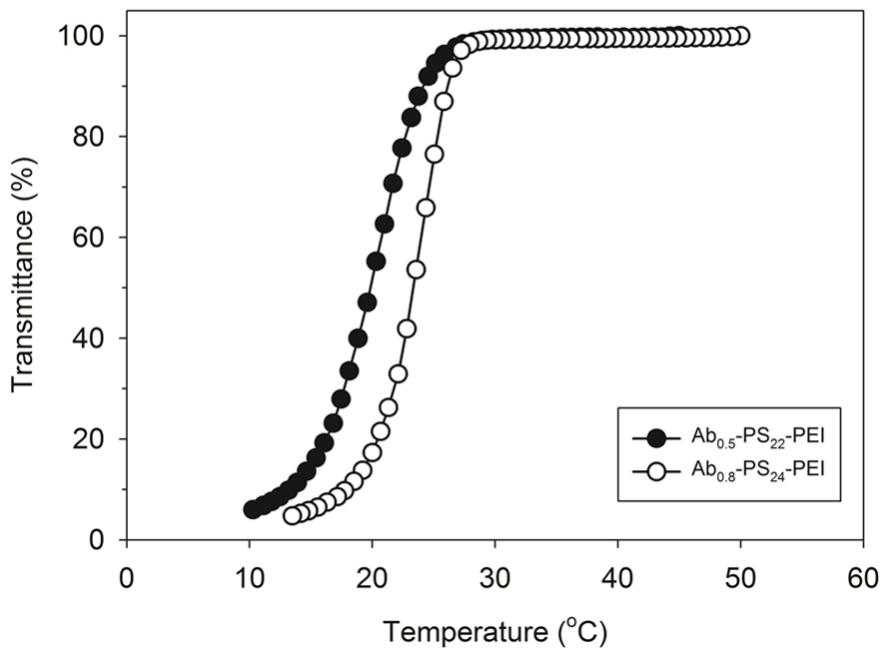

Figure 7. Influence of the Ab substitution degree on the UCST-type phase transition behaviour. (0.5 wt% in water)

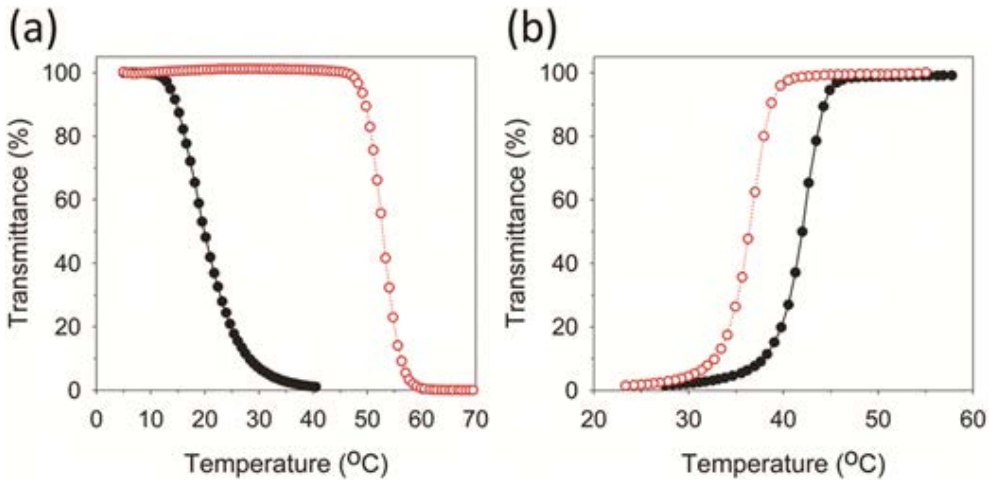

Figure 8. Phase transition of (a) 0.5 wt% Ab_3-Pr_{34}-PEI and (b) 1 wt% $Ab_{0.8}-PS_{24}$-PEI in water before (●) and after (○) UV irradiation.

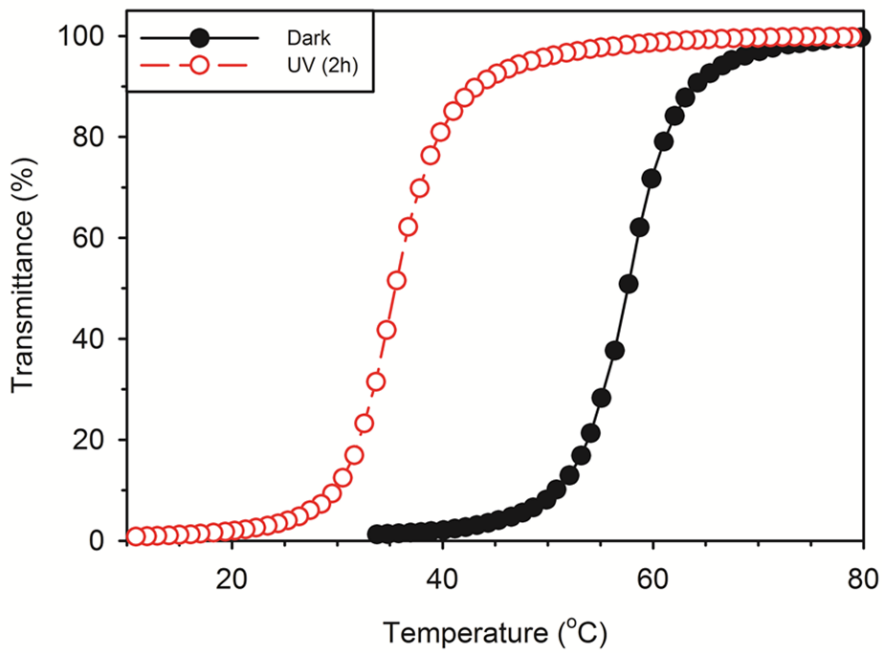

Figure 9. UCST phase transition of 1 wt% Ab_3–PS_{43}–PEI before and after UV irradiation.

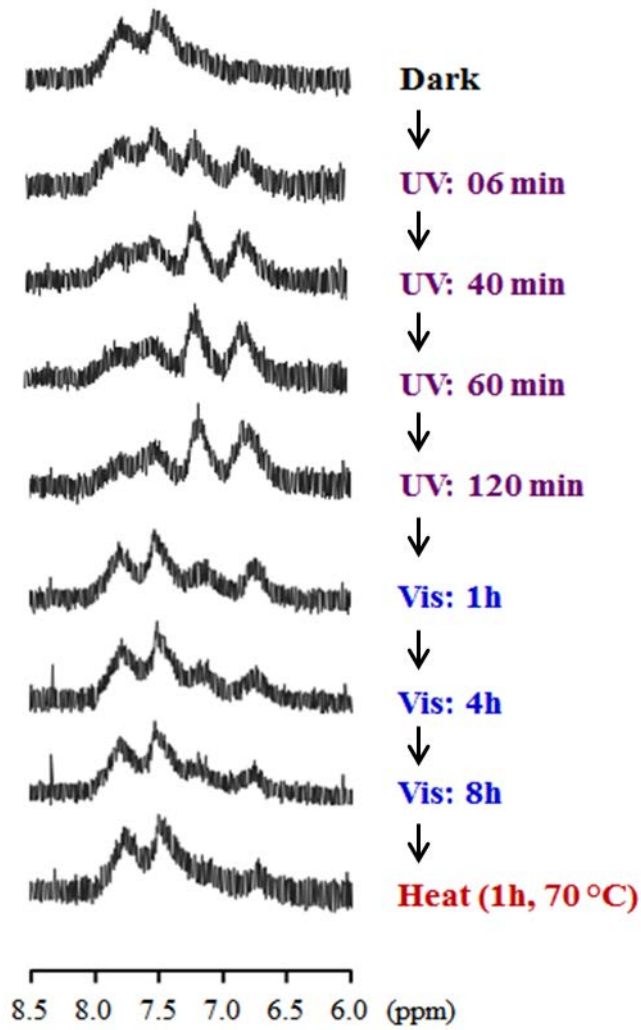

Figure 10. Change in ^{1}H-NMR spectra of Ab_2-Pr_{32}-PEI upon UV and visible irradiation (1 wt% in D_2O).

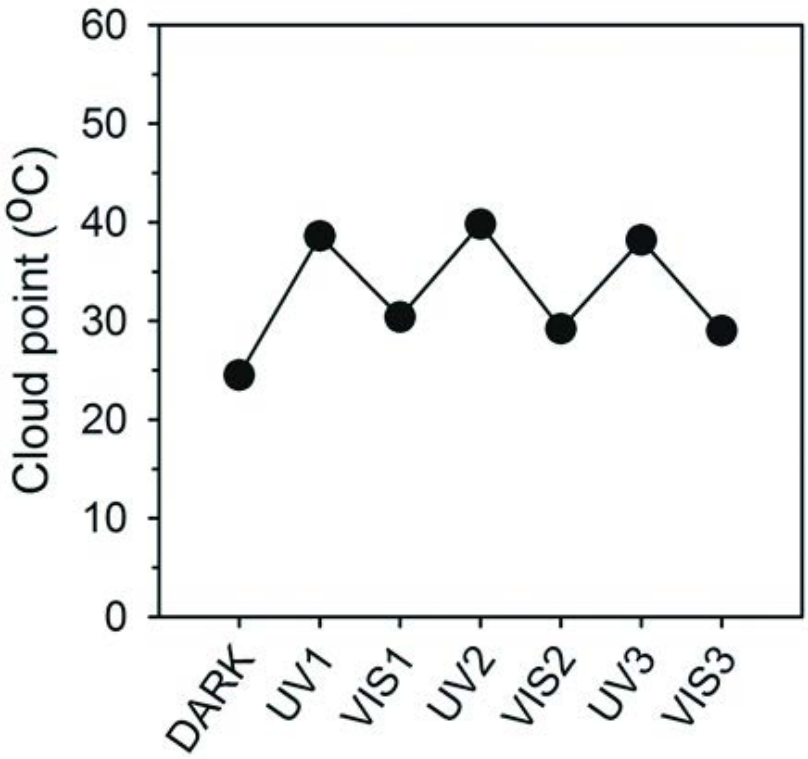

Figure 11. Reversible shifts of LCST phase transition temperature (0.3 wt% Ab_3–Pr_{34}–PEI) upon repeated UV and visible irradiation cycles

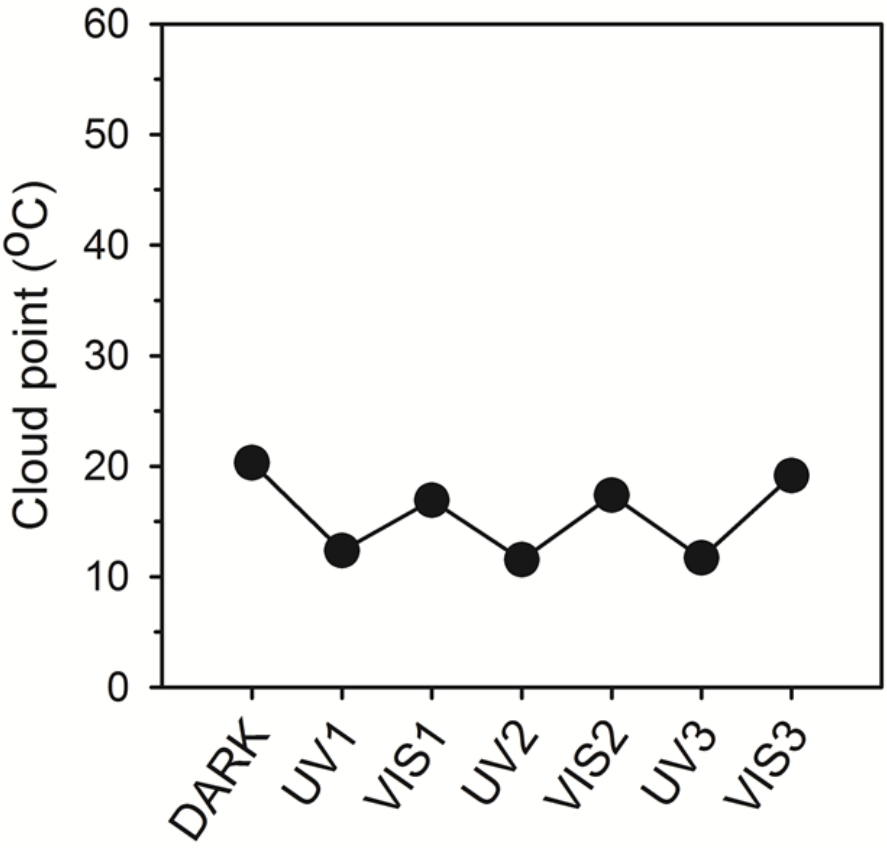

Figure 12. Reversible shifts of UCST phase transition temperature (0.3 wt% Ab_3–Pr_{34}–PEI) upon repeated UV and visible irradiation cycles.

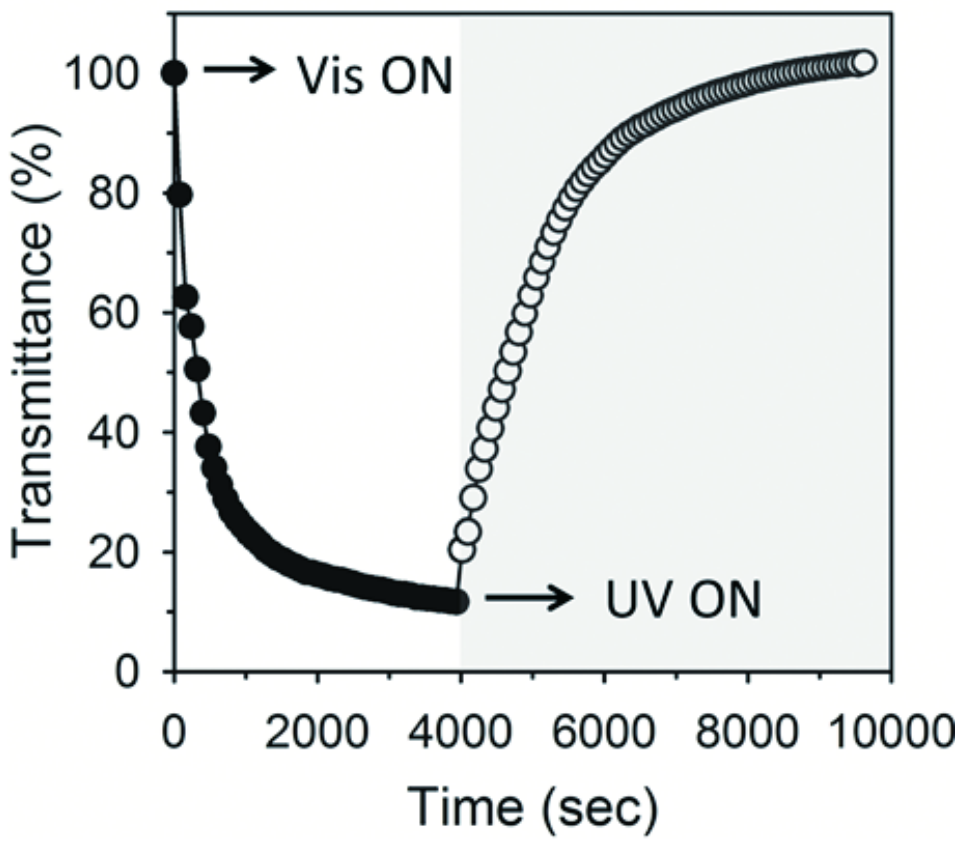

Figure 13. Isothermal phase separation and mixing through sequential visible and UV irradiation (0.3 wt% Ab_3–Pr_{34}–PEI at 36 ℃).

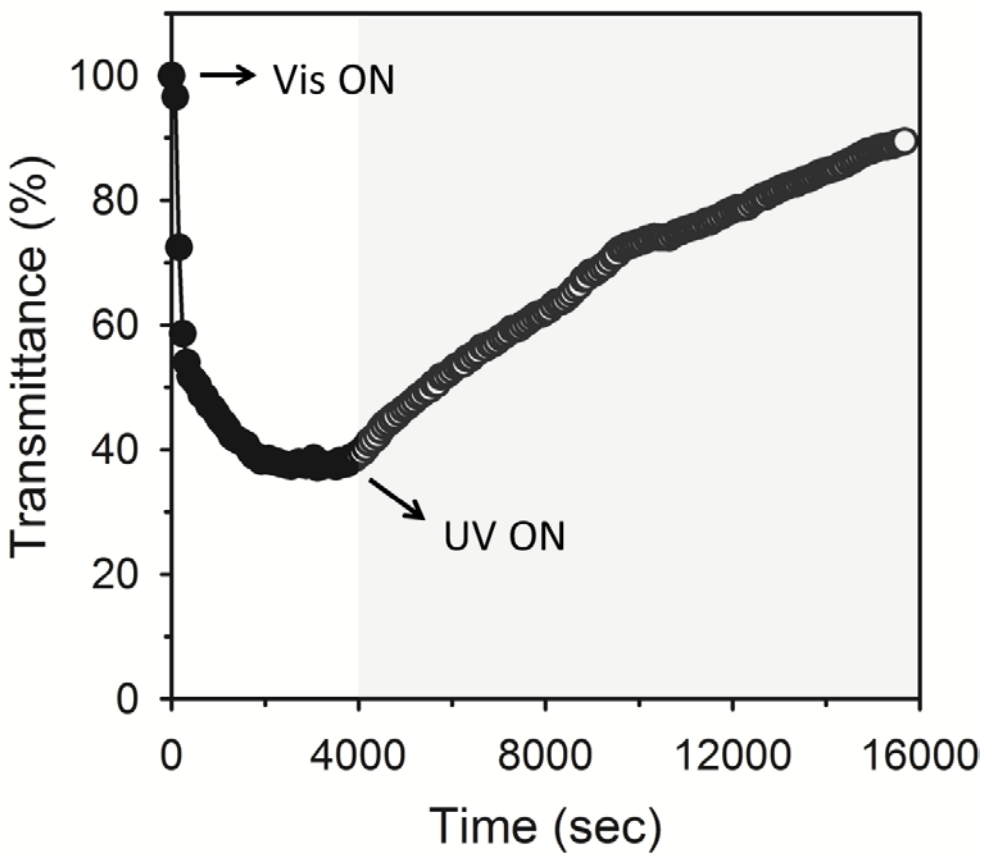

Figure 14. Isothermal phase separation and mixing through sequential visible and UV irradiation.
(0.3 wt% $Ab_{0.8}$–PS_{24}–PEI at 13.5 °C).

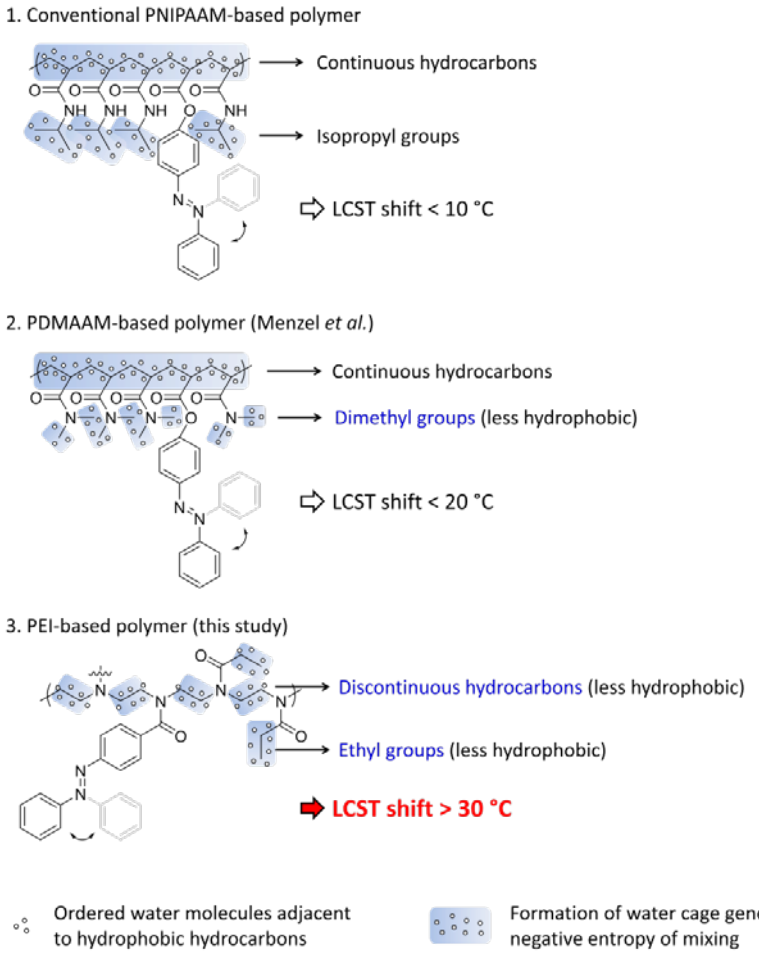

Figure 15. Schematic illustration of three types of light and thermoresponsive polymers for describing the reason of remarkably larger LCST shift of Ab-Pr-PEIs. Water molecules adjacent to hydrophobic groups become well-ordered to form a so-called 'water cage' structure generating more negative entropy of mixing. In case of a conventional poly(*N*-isopropylacrylamide) (PNIPAAM) type polymer (1), contribution of Ab to overall hydrophobicity is relatively small because of hydrophobic isopropyl group near amide bond and continuous hydrocarbon-based backbone. In most reports about the PNIPAAM-based structure, the LCST shift was only several degrees Celsius. Poly(*N*-dimethylacrylamide) type polymer (2) has relatively less hydrophobic dimethyl group. A higher LCST shift up to 20 °C was obtained probably due to the less hydrophobic group with increasing Ab's contribution to total hydrophobicity. Ab-Pr-PEI (3) has discontinuous hydrocarbon backbone with alternating a nitrogen and two carbons, and less hydrophobic ethyl group near the amide bond. This feature may lead larger contribution of Ab to total hydrophobicity and entropy of mixing. Thus, the largest LCST shift could be obtained by the changing the hydrophobicity of Ab by light irradiation.

Product name[b]	Ab[c] feed	Pr[d] or PS[e] feed	Ab content[f]	Pr or PS content[f]	Phase transition type
Ab_2-Pr_{32}-PEI	2.25	37.5[d]	1.67	31.6	LCST
Ab_3-Pr_{34}-PEI	4.50	37.5[d]	2.93	33.6	LCST
$Ab_{0.5}$-PS_{22}-PEI	2.00	25.0[e]	0.46	21.9	UCST
$Ab_{0.8}$-PS_{24}-PEI	3.00	25.0[e]	0.81	24.4	UCST
Ab_3-PS_{43}-PEI	5.00	50.0[e]	3.4	43	UCST

[a]All values indicate mol% to total amine residue in *b*-PEI. [b]Products were named after final contents of substitution. [c]4-phenylazobenzoyl chloride. [d]Propionyl chloride. [e]1,3-Propanesultone. [f]Final contents were calculated based on ^{1}H-NMR.

Table 1. Synthetic information of *b*−PEI derivatives.[a]

Part III. Control of Osmosis and Desalination Driven by Lower Critical Solution Temperature Phase Transition Materials

Chapter 1. Control of Osmosis and Circulatory Desalination Based on *N*-Butyrylated Amine Derivatives

1. Introduction

Water poverty has become a global issue along with increasing desertification and water pollution.[1] Various technologies have emerged to ameliorate these problems, including environmentally-friendly methods to reduce water pollution,[2] recover polluted water,[3] and desalination methods to obtain fresh water from seawater, which accounts for 97% of all the water on Earth.[4] At this time, desalination is at the commercialization stage and more than 40,000,000 m^3 of seawater are being desalinated worldwide every day.[5]

Distillation and reverse osmosis (RO) are the two primary methods used to obtain fresh water from seawater, but forward osmosis (FO) desalination has recently been highlighted due to its high energy efficiency and its lack of a thick semipermeable membrane that resists the high RO pressure (>27 atm).[6] Unlike other methods which require external energy in the form of heat, mechanical or electric energy to overcome the concentration gradient between seawater and fresh water, the FO method uses draw solutions with higher concentrations than seawater (~0.6 M

NaCl equivalent) which can spontaneously 'draw' water from the seawater through a semipermeable membrane. Then the fresh water is recovered from the draw solution by various separation methods.

A pilot scale FO plant is now available using ammonium bicarbonate/ammonium hydroxide (NH_4HCO_3/NH_4OH) as draw solutes.[7] These solutes can be removed from the draw solution to recover fresh water by heating to about 60 ℃, which decomposes the draw solutes into gaseous ammonia (NH_3) and carbon dioxide (CO_2).[8] However, a difficult separation and recovery of the draw solutes are still problems, and FO membranes that are tolerant to the strongly alkaline draw solution are required to prevent membrane fouling, although recently developed polyamide thin film composite (TFC) membranes partially overcome the vulnerability at alkaline pH.[5,9] Various materials such as aluminium sulfate,[10] hydrogel,[11] and magnetic nanoparticles[12] have been examined as substitutes for NH_4HCO_3/NH_4OH draw solute, but they also have difficulties in desalination because complex discontinuous separation of the draw solute is required[10] or only low-salt saline (< 0.035 M NaCl) can be drawn due to the limited drawing power of the draw solution.[11,12] Switchable polarity solvents (SPS) that reversibly convert their polarity using CO2 are also applied to FO desalination in recent reports.[13]

I intended to develop a novel circulatory desalination method driven by a mild temperature gradient using thermoresponsive materials as draw solutes (Fig. 1). Low critical solution temperature

(LCST) materials show an abrupt decrease of solubility above a certain phase transition temperature.[14] Because the osmotic pressure is proportional to the concentration of the solution, the temperature-dependent change of the solubility and effective concentration of LCST mixtures can induce the corresponding change in the osmotic pressure. Below the phase transition temperature, an aqueous solution of LCST materials with a higher concentration than the feed solution, such as seawater or wastewater, can draw fresh water from the feed solution spontaneously by the concentration gradient. The water-drawn LCST mixture is transferred to an environment with a higher temperature than the phase transition temperature. Then, the phase-separated LCST mixture with a decreased effective concentration can release the drawn water into a low-salt solution and return to the low-temperature environment completing the circulatory process.

Since the phase transition temperature of LCST mixtures can be tunable by changing the chemical structure of the LCST materials,[15] the osmotic flow can be controlled by a given temperature gradient, possibly even by mild temperature differences induced by solar or waste heat from power plants and factories.[16] In addition, the separtion, recovery, and reuse of the LCST draw solutes can easily be accomplished by simple circulation of the draw soluton between the high- and low-salt solutions at different temperatures. Moreover, a strongly alkaline pH of the draw solution, which might damage FO membranes, can also be

avoided by controlling the structure of the LCST materials.

In this part, molar mass, aqueous solubility, phase transition temperature, and pH of the draw solution are carefully considered in the design of the molecular structure of the LCST draw solutes. A novel temperature gradient–driven circulatory osmotic process is examined for practical desalination and water purification from high–salt feed solutions including seawater (> 0.60 M NaCl).

2. Experimental Details

2.1. Measurement of osmolality

Osmolality of each draw solute was measured using freezing point depression osmometry (Semi-Micro Osmometer K-7400, Knauer Inc., Germany). Since freezing point depression is only applicable to diluted solution, I measured several points of osmolalities at low concentrations and made correlation diagram to estimate osmolalities of highly concentrated solutions.

2.2. Temperature-controlled water drawing and release

Osmotic flux was measured using handmade glass tubes in a temperature-controlled water bath. The used semi-permeable membranes were made of cellulose triacetate casted onto a non-woven backing consisting of polyester fibers coated with polyethylene (NW-CTA, Hydration Technology Innovation (HTI), USA). The membrane (diameter: 3.3 cm) was placed in the middle of upper and below tubes, and each tube was filled with a NaCl solution and an LCST mixture with stirring, respectively. The selective layer of the semipermeable membrane faced the LCST mixture. The osmotic water flux from the NaCl solution to the LCST mixture was calculated from the volumetric change of each solution during 1 h after 1 h of stabilization at 18 (±2) °C. The reversed osmotic flux from the LCST mixture to the NaCl solution was

similarly calculated at 55 (±2) ℃.

2.3. Circulatory osmotic desalination by a temperature gradient

The circulatory desalination unit consisted of two sets of glass tubes at different temperatures (18(±2) ° C and 55(±2) ° C). In the low temperature drawing set, a high-salt solution and an LCST mixture filled each glass tube. In the high temperature recovery set, an LCST mixture and a low-salt solution filled each glass tube. The drawing and recovery sets were connected to each other with silicone rubber tubes. The LCST mixture circulated between the two sets by a peristaltic pump. The osmotic desalination flux was calculated from the volumetric change of each salt solution.

Circulatory desalination was performed using an *n*Bu-TAEA (1.6 M) solution between 0.6 M and 0.15 M NaCl solutions for the first desalination unit, and an *n*Bu-PEI (0.37 M) solution between 0.15 M and 0.075 M NaCl solutions for the second desalination unit. Every solution in each unit was stirred during measurement.

The permeation of the solute molecules through the membrane was determined using HPLC. The permeation percentage of solute A ($\%P_A$) was calculated by the following equation:

$$\%P_A = \frac{C_A' \times V}{C_A \times v} \times 100$$

where C_A is the initial concentration of A solution, v is the

volume of permeated water, C_A' is the concentration of A on the other side of the membrane after osmosis, and V is the volume of the solution on the other side of the membrane. The rejection efficiency was defined as $(100 - \%P_A)$.

3. Results and Discussion

3.1. Temperature-controlled water drawing and release by *n*Bu-TAEA and *n*Bu-PEI

My desalination method is based on water drawing from high-salt solutions by the LCST mixtures at low T and water release from the LCST mixtures to low-salt solutions at high T. As the effective concentrations of the LCST mixtures changed abruptly during the phase separation, the osmotic pressure changed correspondingly and water molecules were drawn into and released from the LCST mixtures. For efficient and practical desalination, the drawable concentration of the high-salt solution should be maximized and the releasable concentration of the low-salt solution should be minimized, which are determined by the effective concentrations of the LCST mixtures at low and high T.

To determine the maximum drawable concentration, the osmotic flux from NaCl solutions with various concentrations to the LCST mixtures was measured at 18 ° C, a lower temperature than the phase transition temperature of LCST mixtures (Fig. 2). Highly concentrated *n*Bu-TAEA mixtures over 2.4 M can be prepared given their low molar mass and high aqueous solubility. The osmotic flux was positively related to the concentration gradient between NaCl solutions and *n*Bu-TAEA mixtures (Fig. 2b). It was notable that 2.0 M *n*Bu-TAEA mixtures could draw water from a 0.60 M NaCl solution, a seawater equivalent, which was hardly drawable by

other draw solutions in previous reports.[11,12] As for *n*Bu-PEI with a rather higher molar mass, solutions around 0.50 M can be readily obtained. The concentration gradient-osmotic flux relationship was almost similar to the *n*Bu-TAEA system (Fig. 2d). As an *n*Bu-PEI mixture over 0.4 M could draw a 0.15 M NaCl solution (i.e., a physiological saline), this *n*Bu-PEI mixture might be used to purify various types of polluted solutions with low concentrations of heavy metals or microbes,[6] although it could not draw water directly from seawater. These drawing powers are related with their osmolalities, which could be measured by freezing point depression. The osmolality of each draw solutes were determined (Fig. 3). At low concentration, osmolalities were proportional to molalities for both *n*Bu-TAEA and *n*Bu-PEI. Osmolality at higher concentration was calculated through extrapolation since freezing point depression is only applicable to dilute solution; they could not be reliably measured using osmometer. Osmolality of 2.0 M (7.2 m) *n*Bu-TAEA solution was 6.0 Osm/kg which could make water drawing from seawater (~1.2 Osm/kg). Osmolality of 0.49 M (1.2 m) *n*Bu-PEI solution was 2.1 Osm/kg which could make water drawing from physiological saline water (~0.30 Osm/kg).

However, water fluxes were not fast compared to those osmotic pressure differences and even 0.49 M *n*Bu-PEI (2.1 Osm/kg) cannot draw seawater. This could be because of concentration polarization phenomenon which comes from lowering of actual osmotic pressure difference because of accumulation of feed

solutes and dilution of draw solution very near the membrane.[6] My draw solutes – especially bigger one, *n*Bu–PEI – are large organic molecules, thus their mobility in aqueous condition could be slower than those of small ions such as Na^+ and Cl^-, thus their practical osmotic pressure could be smaller than calculated values. Also, I used small scale test units for flux measurements since large quantity of synthetic materials are not easy to be prepared in laboratory. If the draw solutes are applied into large scale FO system which uses cross–flow type operation, enhanced osmotic fluxes could be probably generated. More detailed studies should be required.

Next, the minimum releasable concentration was determined by measuring the osmotic flux from the phase–separated LCST mixtures to NaCl solutions at 55 ° C, a higher temperature than the phase transition temperature (Fig. 2c and e). Because the effective concentration of the upper water–rich phase of the LCST mixture was far lower than the initial concentration, the upper phase could release water into NaCl solutions with significantly lower ionic concentrations than the initial concentration of the feed solution.

The osmotic flux increased as the concentration of the NaCl solution increased. It was also noteworthy that *n*Bu–TAEA mixtures could release water into a 0.15 M NaCl solution at 55 ° C (Fig. 2c). *n*Bu–PEI mixtures could even release water into a 0.050 M NaCl solution at 55 ° C (Fig. 2e). To understand those water release effect, the osmotic pressures of water–rich phases in the LCST mixtures were also evaluated. Firstly, I measured

concentration of *n*Bu-TAEA and *n*Bu-PEI in water-rich phase of each solution at 55 ° C using ^{1}H-NMR spectrometry (Table 1). The concentrations of water-rich phases in 1.0 M *n*Bu-TAEA and 0.24 M *n*Bu-PEI were 0.22 M (0.24 m) and 0.052 M (0.056 m), which are equal to 0.22 Osm/kg and 0.077 Osm/kg, respectively. These osmolality values were calculated from the equations in Fig. 3. Since these values are lower than 0.15 M (~0.30 Osm/kg) and 0.050 M (~0.10 Osm/kg) NaCl solutions, respectively, water could be released to these NaCl solutions, which become productive water.

Therefore, low-molar-mass *n*Bu-TAEA mixtures could be useful for drawing water directly from high-salt solutions such as seawater at low T. After drawing, phase-separated *n*Bu-TAEA mixtures could release water into NaCl solutions with concentrations of around 0.15 M. On the other hand, high-molar-mass *n*Bu-PEI mixtures could be useful for drawing water from relatively low-salt solutions with concentrations around 0.15 M, but they could produce more diluted solutions. The difference of molar mass of two LCST solutes also influenced the permeation of the solutes across the membrane. By using NW-CTA membrane of HTI, *n*Bu-TAEA showed low permeation (2.0%) or high rejection (98%), which is equal to that of Na^{+} ion (Table 1). High-molar-mass *n*Bu-PEI showed even higher rejection efficiency (99.6%), probably due to its larger hydrodynamic volume. Semipermeable membranes with higher rejection efficiencies and osmotic flux would be welcomed for future practical FO desalination methods using *n*Bu-TAEA or *n*Bu-PEI.[17]

Furthermore, the successive combination of an *n*Bu–TAEA desalination unit and an *n*Bu–PEI unit could possibly produce low–salt water directly from seawater, considering the maximum drawable and releasable concentrations of both LCST solutes. This possibility will be discussed in the last section.

3.2. Circulatory desalination by temperature gradient

After determining the maximum drawable and minimum releasable concentrations of the salt solutions, I performed temperature gradient–driven circulatory osmotic desalination using homemade glass tubes at different temperatures (Fig. 4a). In this desalination system, LCST mixtures circulate between low T and high T units for the drawing, transfer and release of water. A high–salt feed solution faces the LCST mixtures across a semipermeable membrane in a low T–drawing set, and a low–salt solution faces the LCST mixtures in a high T–recovery set. For better visualization of the desalination process, I stained the high salt solution with Evans blue, and the low salt solution with Congo red (Fig. 4b).

Based on the drawable and releasable concentration data, the *n*Bu–TAEA mixture was used for desalination from a 0.60 M NaCl solution to a 0.15 M NaCl solution. After drawing water from the 0.60 M NaCl solution at low T, the *n*Bu–TAEA mixture was transported to the high T recovery set. At the high T set, the *n*Bu–TAEA mixture phase–separated rapidly into the upper phase with a low *n*Bu–TAEA concentration and the lower phase with a high

*n*Bu−TAEA concentration. The upper phase directly contacted the semipermeable membrane, and released water into the 0.15 M NaCl solution. The drawing and release of water was synchronized via the circulation process of the LCST mixture. More importantly, this circulatory system automatically recovers the draw solutes based on the phase separation and sedimentation. During circulation, only the lower phase with a high concentration of *n*Bu−TAEA could be transported to the low T− drawing set because the linking silicon tube was connected at the bottom of the high T−recovery set. The high concentration of *n*Bu−TAEA and volume of the draw solution at the drawing set could be maintained by recovery. The drawing and release of water as w ell as the recovery and re−dissolving of the draw solutes took place simultaneously in the circulation process, unlike other FO systems consisting of separate and rather complicated drawing and recovery processes.[8,10−12]

Using circulatory desalination, the 1.6 M *n*Bu−TAEA mixture successfully desalinated 0.60 M NaCl solution into 0.15 M (Fig. 4c). Similar values were observed in both drawing and releasing fluxes. The desalination flux was maintained for almost 50 h, which also supported the stability of the semipermeable membrane. As for the high−molar−mass *n*Bu−PEI mixture (0.37 M), it showed successful desalination from 0.15 M to 0.075 M (Fig. 4d). The lowering of the blue high−salt solution and the rising of the red low−salt solution are clearly visualized. As expected, a higher drawing flux was observed compared to the release flux in the *n*Bu−PEI−based desalination (Fig. 2d−e). Interestingly, the drawing flux of the 0.37

M *n*Bu-PEI mixture from the 0.15 M NaCl in the circulatory system (Fig. 4d) was around 0.6 LMH, significantly higher than the drawing flux (0.14 LMH) of the 0.41 M *n*Bu-PEI mixture from the 0.15 M NaCl in the simple osmotic system (Fig. 2d). This difference was probably due to the concentration gradient or uneven distribution of *n*Bu-PEI solutes between the low T and high T sets, which might be generated by the recovery of the highly concentrated lower phase of the *n*Bu-PEI mixture. The concentration gradient would be helpful for more efficient drawing from a high-salt solution and easier release into a low-salt solution in the circulatory desalination process.

3.3. Successive desalination via combination of circulatory osmotic systems based on low- and high-molar-mass LCST draw solutes

Considering that drawing, transfer, and release of water and even separation and recovery of draw solutes proceed simultaneously in my circulatory desalination system, and that the low-molar-mass *n*Bu-TAEA has a high drawing power from a high-salt solution and the high-molar-mass *n*Bu-PEI shows efficient release into a low-salt solution and a high rejection efficiency, I suggested a successive desalination method through a linear combination of two circulatory osmotic systems. As illustrated in Fig. 5, the desalinated water from the first circulatory desalination unit using a low-molar-mass LCST mixture could be

directly treated by the second unit using a high-molar-mass LCST mixture. In this way, a high-salt-solution such as seawater could be desalinated into a mild-salt-solution by a low-molar-mass LCST mixture with high drawing power, and the mild-salt-solution could be successively desalinated to produce a low-salt- solution by a high-molar-mass LCST mixture. Since a seawater equivalent (0.60 M) could be desalinated into a 0.15 M NaCl solution through the *n*Bu-TAEA-based circulatory unit, the produced solution could be successively desalinated into a lower-salt-solution through the *n*Bu-PEI-based unit. Due to the high rejection efficiency of the high-molar-mass draw solute, it would be expected to produce water with higher purity. Of course, the modulation of osmotic flow would be required considering the different flux of each unit. Furthermore, this concept can be expanded to the linear combination of more than two circulatory desalination systems using draw solutes with different molar masses in an adequate manner for efficient and high-quality desalination or purification of solutions with various degrees of concentrations or contamination.

4. Conclusions

To overcome the weaknesses of current desalination techniques, I developed a novel circulatory FO desalination system driven by a mild temperature gradient based on LCST materials. Drawing, transfer, release, and recovery proceeded simultaneously in the circulatory osmotic system. Of course, separation using RO or ultrafiltration (UF) is also possible since aggregated draw solution in high T has much lowered osmotic pressure. However, I focused on achievement of continuous process. To the best of my knowledge, this system is the first FO process showing synchronized water drawing, solute recovery, and generation of productive water. Temperature gradient was only main factor for energy efficiency. Considering that the molar mass, phase transition temperature and aqueous solubility of LCST draw solutes can be delicately controlled by molecular structure design, further optimization of the draw solute is possible for a more practical FO system. The low osmotic flow should be partially overcome by the development of draw solutes with lower hydrodynamic volume and higher diffusion coefficient because the osmotic flux is closely related with internal concentration polarization of solutes in the membrane layer.[8] Switchable polarity solvents which reversibly convert their polarity mostly triggered by CO_2 are also good candidates for circulatory FO desalination, since they can be separated from aqueous solution into liquid/liquid forms by 1-step stimuli.[18] In addition, the desalination efficiency could be greatly

enhanced by using newly developed membranes based on carbon nanotubes,[19] graphenes,[20] nanofibers,[21] or aquaporins[22]. Moreover, direct desalination from high-salt seawater into low-salt water, even at the level of fresh water (< 0.017 M), could be attainable by the successive combination of circulatory desalination systems. In the near future, various materials with stimuli-sensitivity, including temperature-, light-, or ionic strength-sensitivity, have great potential to solve water or energy problems by synergetic combination with osmotic control or membrane technologies

5. References

[1] J. F. Reynolds, D. M. Stafford Smith, E. F. Lambin, B. L. Turner, M. Mortimore, S. P. J. Batterbury, T. E. Downing, H. Dowlatabadi, R. J. Fernandez, J. E. Herrick, E. Huber-Sannwald, H. Jiang, R. Leemans, T. Lynam, F. T. Maestre, M. Ayarza and B. Walker, *Science*, 2007, 316, 847; C. J. Vörösmarty, P. B. McIntyre, M. O. Gessner, D. Dudgeon, A. Prusevich, P. Green, S. Glidden, S. E. Bunn, C. A. Sullivan, C. Reidy Liermann and P. M. Davies, *Nature*, 2010, 467, 555.

[2] P. Anastas and N. Eghbali, *Chem. Soc. Rev.*, 2010, 39, 301.

[3] M. A. Shannon, P. W. Bohn, M. Elimelech, J. G. Georgiadis, B. J. Mariñas and A. M. Mayesas, *Nature*, 2008, 452, 301.

[4] R. F. Service, *Science*, 2006, 313, 1088.

[5] Q. Schiermeier, *Nature*, 2008, 452, 260; M. Elimelech and W. A. Phillip, *Science*, 2011, 333, 712.

[6] R. E. Karavath and J. A. Davis, *Desalination*, 1975, 16, 151; T. Y. Cath, A. E. Childress and M. Elimelech, *J. Membr. Sci*, 2006, 281, 70.

[7] R. L. McGinnis, N. T. Hancock, M. S. Nowosielski-Slepowron, G. D. McGurgan, *Desalination*, 2013, 312, 67.

[8] J. R. McCutcheon, R. L. McGinnis and M. Elimelech, *Desalination*, 2005, 174, 1; J. R. McCutcheon, R. L. McGinnis and M. Elimelech, *J. Membr. Sci.*, 2006, 278, 114.

[9] J. E. Miller, L. R. Evans, *Sandia Report*, SAND2006-4634, Sandia National Laboratories, California, 2006; R. Wang, L. Shi,

C.Y.Y. Tang, S.R. Chou, C. Qiu and A.G. Fane, *J. Membr. Sci.*, 2010, 355, 158; N. Ma, J. Wei, R. Liao and C. Y. Tang, *J. Membr. Sci.*, 2012, 405-406, 149.

[10] Z. Liu, H. Bai, J. Lee and D. D. Sun, *Energy Environ. Sci.*, 2011, 4, 2582.

[11] D. Li, X. Zhang, J. Yao, Y. Zeng, G. P. Simonb and H. Wang, *Soft Matter*, 2011, 7, 10048; D. Li, X. Zhang, J. Yao, G. P. Simonb and H. Wang, *Chem. Commun.*, 2011, 47, 1710.

[12] M. M. Ling, K. Y. Wang, and T.-S. Chung, *Ind. Eng. Chem. Res.*, 2010, 49, 5869.

[13] P. G. Jessop, S. M. Mercera and D. J. Heldebrant, *Energy Environ. Sci.*, 2012, 5, 7240; M. L. Stone, C. Rae, F. F. Stewart and A. D. Wilson, *Desalination*, 2013, 312, 124

[14] R. B. Griffiths and J. C. Wheeler, *Phys. Rev. A*, 1970, 2, 1047.

[15] H. Kim, S. Lee, M. Noh, S. H. Lee, Y. Mok, G. Jin, J.-H. Seo and Y. Lee, *Polymer*, 2011, 52, 1367.

[16] M. Noh, Y. Mok, S. Lee, H. Kim, S. H. Lee, G. Jin, J.-H. Seo, H. Koo, T. H. Park and Y. Lee, *Chem. Commun.*, 2012,48, 3845.

[17] H. G. Schild, Prog. Polym. Sci., 1992, 17, 163.

[18] M.T. M. Pendergast and E. M.V. Hoek, Energy Environ. Sci., 2011, 4, 1946.

[19] H. G. Park, F. Fornasiero, J. K. Holt, C. P. Grigoropoulos and O. Bakajin, Nano Today, 2007, 2, 22.

[20] D. Cohen-Tanugi and J. C. Grossman, Nano Lett., 2012, 12, 3602.

[21] X. Song , Z. Liu and D. D. Sun, Adv. Mater., 2011, 23, 3256.

[22] M. Kumar, M. Grzelakowski, J. Zilles, M. Clark and W. Meier, Proc. Natl. Acad. Sci. U.S.A., 2007, 104, 20719.

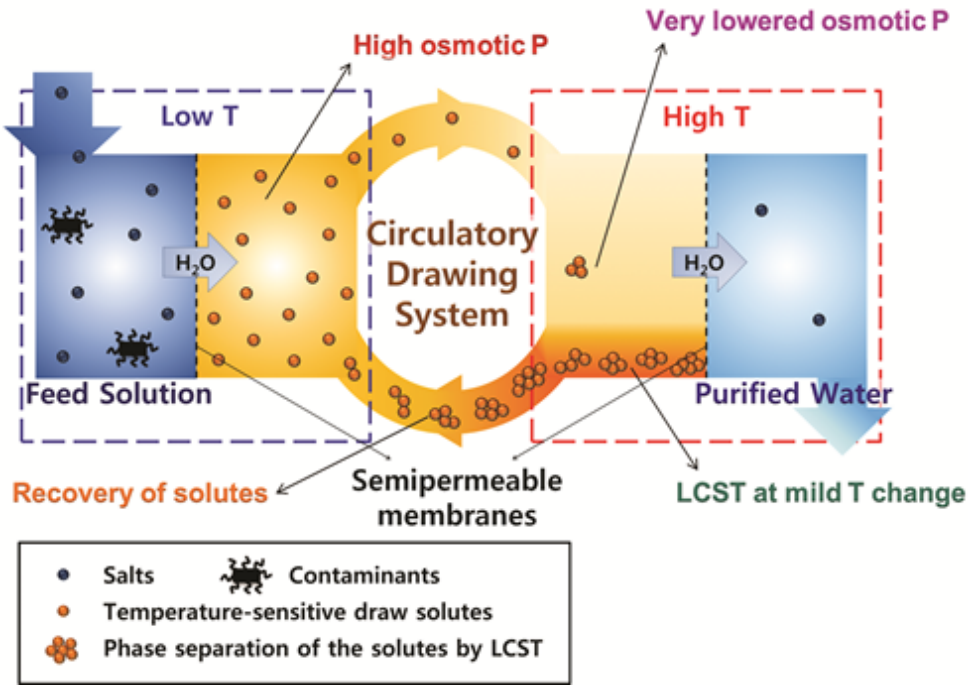

Figure 1. Simplified scheme of circulatory osmotic desalination based on LCST phase transition.

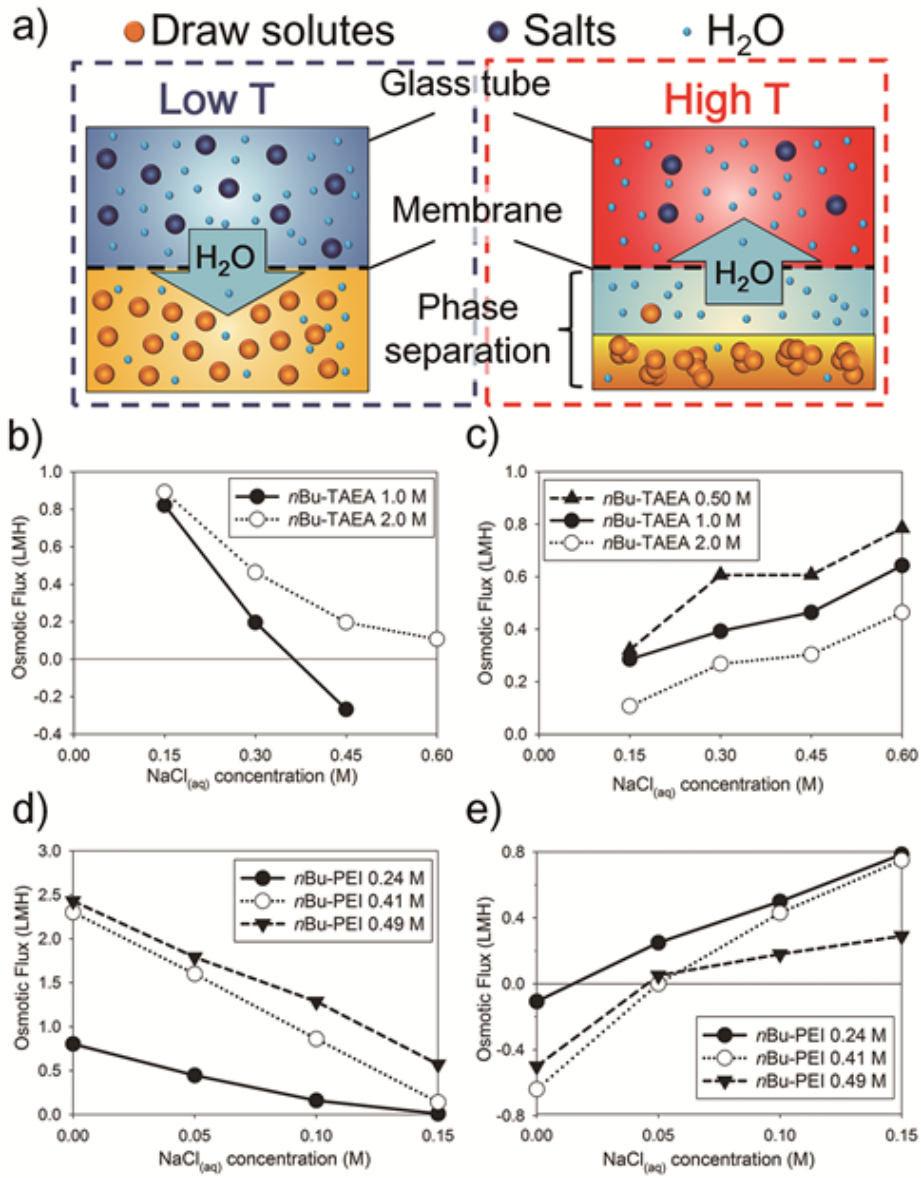

Figure 2. a) Illustration of glass tubes to measure temperature controlled osmosis and fluxes. Osmotic fluxes b) from NaCl solutions to *n*Bu-TAEA mixtures at low T, c) from *n*Bu-TAEA mixtures to NaCl solutions at high T, d) from NaCl solutions to *n*Bu-PEI mixtures at low T, and e) from *n*Bu-PEI mixtures to NaCl solutions at high T.

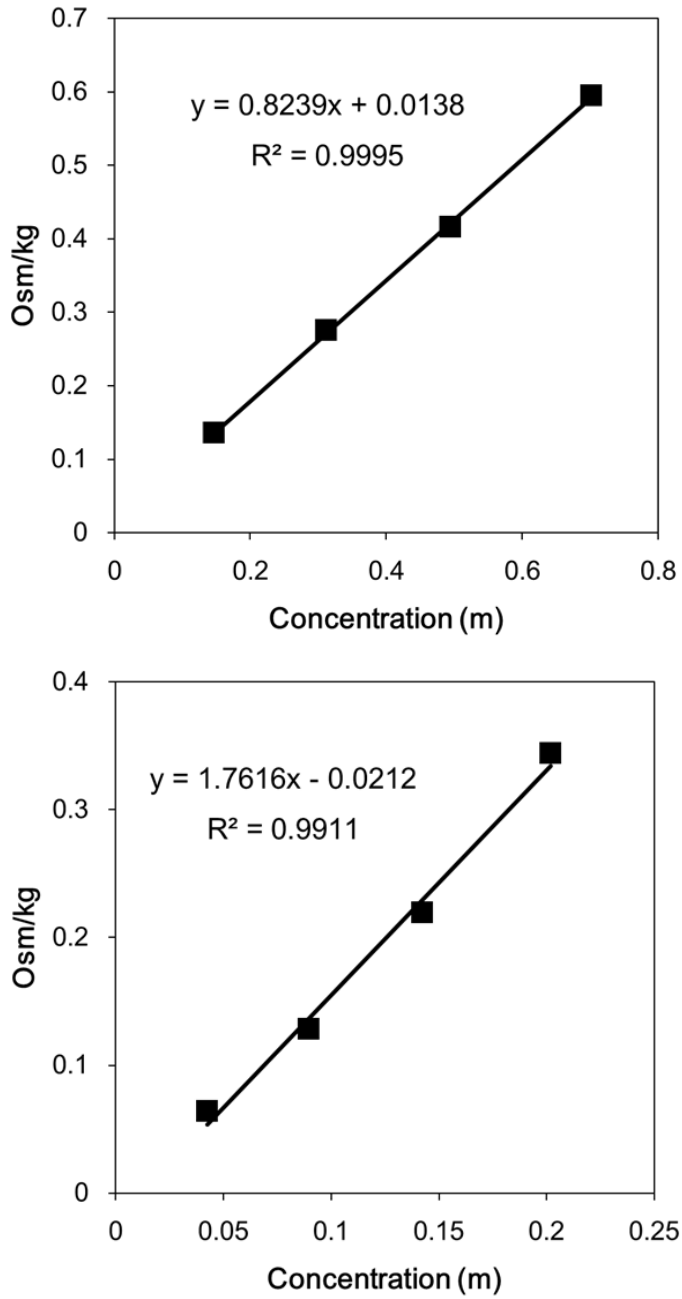

Figure 3. Osmotic pressure of *n*Bu-TAEA (up) and *n*Bu-PEI (down) measured by freezing point depression.

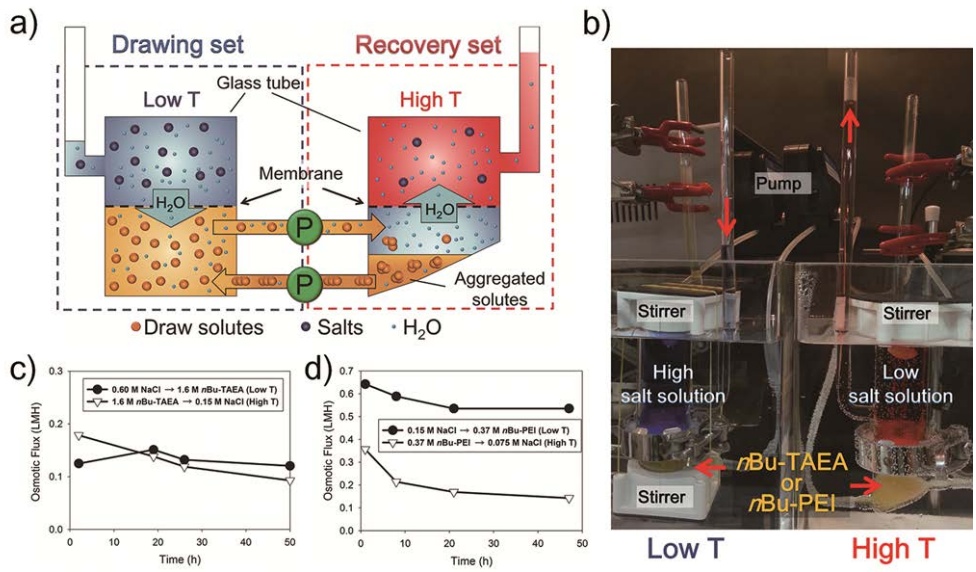

Figure 4. a) Schematic diagram of a temperature-gradient driven osmotic desalination unit. b) A picture of the desalination unit. The high-salt solution was stained with a blue dye, and the low-salt unit was stained with a red dye. c) The desalination flux from 0.60 M NaCl to 0.15 M NaCl through 1.6 M *n*Bu-TAEA desalination unit. d) The desalination flux from 0.15 M NaCl to 0.075 M NaCl through 0.37 M *n*Bu-PEI desalination unit.

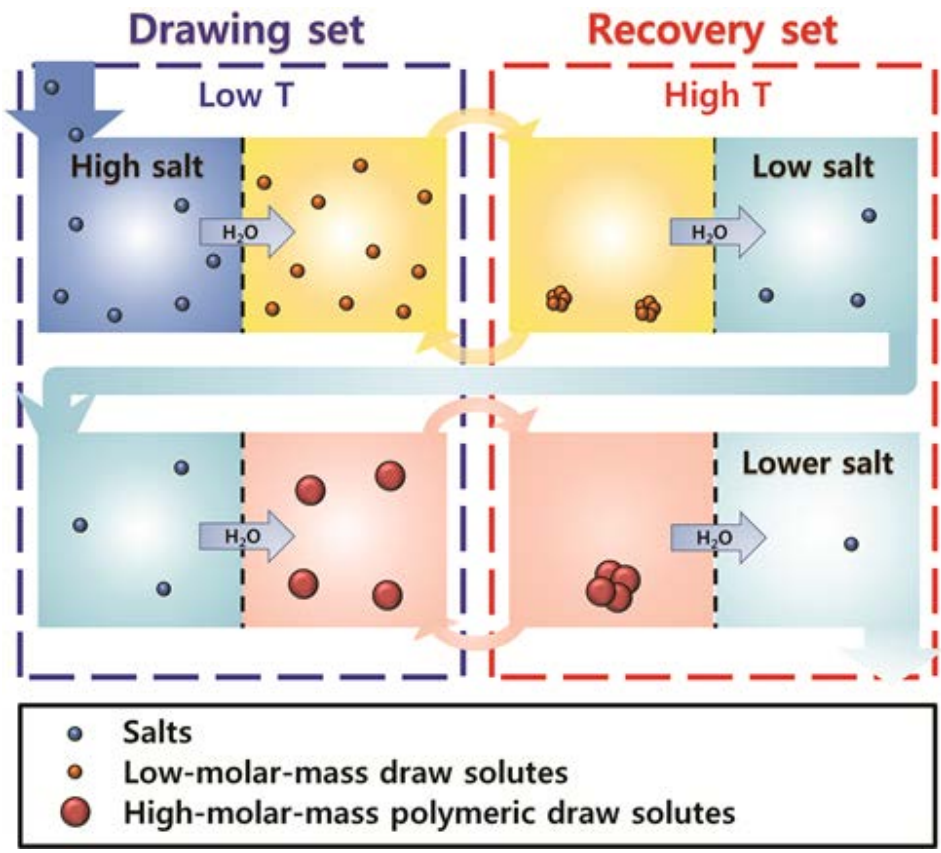

Figure 5. Schematic illustration of a possible successive osmotic desalination system. A low-molar-mass LCST draw solute-based circulatory desalination unit can be linearly combined with a high-molar-mass LCST draw solute-based circulatory desalination unit for the production of low-salt water with high purity from high-salt water.

Draw solutes	M (g mol^{-1})	Solubility (wt%)	Molarity[b] (mol L^{-1})	Phase transition temp. (°C)	Residual solute concentrations in the water-rich phase[c] (mol L^{-1})	Rejection efficiency[d] (%)
*n*Bu-TAEA	356	>80	>2.4	32 (1.0 M)	0.22	98.0
*n*Bu-PEI	1238[a]	>70	>0.57	31 (0.24 M)	0.052	99.6

[a] The molar mass of *n*Bu-PEI was derived from number-averaged molecular weight (M_n) determined by the ^{1}H-NMR spectrum. [b] The molarity was calculated on basis of the density at 25 °C. [c] After phase separation at 55 °C. [d] Rejection of solutes by the membrane. NaCl rejection efficiency was 98.4% under the same conditions.

Table 1. Physicochemical characteristics of *n*Bu−TAEA and *n*Bu−PEI.

Chapter 2. Forward Osmotic Control Driven by Glycol Ethers.

1. Introduction

Earth is facing an impending water shortage due to increasing water pollution and progressing desertification.[1] Seawater, which accounts for 97% of all the water on Earth, is an attractive source of potential fresh water, and more than 40,000,000 m^3 of seawater are desalinated worldwide every day.[2] Distillation and reverse osmosis (RO) are the two primary methods for obtaining fresh water, but forward osmosis (FO) is an emerging technique for energy-efficient desalination.[3] The FO method uses a draw solution with a higher concentration than the feed solutions, *i.e.*, seawater, which can spontaneously 'draw' fresh water from the feed solution through a semipermeable membrane. Fresh water can be recovered from the diluted draw solution following the removal of the draw solute by various methods.

A FO system employing ammonium bicarbonate/ammonium hydroxide (NH_4HCO_3/NH_4OH) as draw solutes has been extensively studied for practical desalination applications (Fig. 1, left).[4] After withdrawing water from the feed solutions, the draw solutes decompose into ammonia (NH_3) and carbon dioxide (CO_2), which exhibit liquid-gas (L-G) phase separation from water upon heating

to approximately 60 °C. The NH_4HCO_3/NH_4OH–based FO system is now in the pilot stage, but several problems must be overcome to achieve distillation and RO in practical desalination applications.[5] For example, the decomposition step requires considerably elevated temperatures, the separation and recovery of the gaseous draw solutes require complex equipment for distillation and re-condensation, and the strongly basic pH of the draw solution can potentially damage the semipermeable membrane although thin film composite (TFC) membranes comprising a polyamide selective layer have recently been developed and partially overcome the vulnerability at the basic conditions.[6] Various materials, including inorganic salts,[7] magnetic nanoparticles,[8] and hydrogels,[9] have been explored as substitutes for NH_4HCO_3/NH_4OH, but these materials require complex discontinuous desalination processes or exhibit very limited osmotic drawing powers that allow only limited water withdrawal, even from low-salt saline solutions (<0.035 m NaCl).

There are several requirements for an ideal draw solute. First, the solute should exhibit high aqueous solubility to achieve high drawing powers because the osmotic pressure (π) is related to the molality of the solution (m), as described by a virial expansion of the Morse equation (1):

$$\pi = \rho RT\ (m + Bm^2 + Cm^3 + \cdots) \qquad (1)$$

where ρ is density, R is the gas constant, T is temperature, B is

the osmotic second virial coefficient and C is the osmotic third virial coefficient. Second, the solute should possess a low molar mass because the molar mass is inversely related to the molality or osmotic pressure except for polyelectrolyte molecules with a large amount of counter-ions. Third, the draw solutes should be separated by mild temperature changes, preferably induced by waste heat or sunlight. Fourth, the separation and recovery should be simple and efficient, and residual draw solute should be minimised in the separated water. Fifth, it will be more acceptable if the draw solution exhibits neutral pH values to reduce potential damages to the membrane.

In my study, I aimed to develop a FO system employing draw solutes with the desirable characteristics mentioned above (Fig. 1, right). Lower critical solution temperature (LCST) materials[10] were selected as candidates for the draw solutes. At temperatures below the phase transition temperature, LCST materials are miscible with water at high concentrations, enabling the efficient withdrawal of water from feed solutions. The water-drawn solution is subsequently transferred to an environment at a higher temperature than the phase transition temperature. At this elevated temperature, the LCST material exhibits liquid-liquid (L-L) phase separation from water, reducing the effective concentration of the draw solution. The phase-separated draw solution with a decreased effective concentration can then spontaneously release water into a low-salt solution. Because the phase transition temperature of LCST materials can be controlled by altering the chemical

structure,[11] the energy requirement for the separation of draw solutes can be greatly reduced by using a LCST material with a low phase transition temperature. Moreover, the L–L phase–separated LCST material can be recovered into the original draw solution through a simple liquid–liquid separator without the need for a complex re–condensation process of gaseous draw solutes. It was recently reported that a desalination method through L–L phase separation of switchable polarity solvents, but gaseous CO_2 was also required as a stimuli for the polarity change.[12]

In my previous report, I demonstrated that the osmotic pressure can be effectively controlled by the LCST phase transition of a low–molar–mass *N*–acylated amine derivative.[13] In this study, I suggest glycol ethers (GEs) as suitable draw solutes for FO. Many low–molar–mass GEs are miscible with water at all concentrations below the phase transition temperature,[14] allowing the generation of sufficient osmotic pressure to draw water from seawater. These GEs can be phase–separated at approximately 30 °C, which is significantly lower than the decomposition temperature of ammonium bicarbonate.[4] Aqueous solutions of GEs with hydroxyl– and ether–based structures exhibit neutral pH values, reducing the potential damage to the membrane. In addition, the low viscosities of GEs[15] can be beneficial in establishing circulation processes,[16] and their facile synthesis makes them amenable to commercialisation.

By evaluating the thermoresponsive L–L phase separation of different GE/water mixtures, I examined the use of GEs as draw

solutes in detail. In particular, the effective concentration or osmolality was analyzed in the GE/water mixture to compare the power of osmotic withdrawal, water flux, and the final salt concentration of the resulting water.

2. Experimental Details

2.1. Measurement of osmolality

The osmolality of the DEH/water mixture at various concentrations was measured using freezing point depression osmometry (Semi-Micro Osmometer K-7400, Knauer Inc., Germany) and vapor pressure depression osmometry (Vapor Pressure Osmometer K-7000, Knauer Inc., Germany). In case of the vapor pressure osmometry, the osmolalities of the samples were measured at 30 ° C, 40 ° C, and 50 ° C.

2.2. Temperature-controlled water withdrawal and release

FO flux experiments were performed using cross-flow circulating module referring to Cath *et al.*[17] The glass cell consists of two channels; one on each side of the cellulose triacetate membrane (Hydration Technology Innovation, USA). Feed and draw solution flowed concurrently through respective cell at the same flow rate of 700 mL/min. The selective layer of the semipermeable membrane faced the GE solution. The osmotic water flux from the NaCl solution to the GE solution was calculated from the weight change of each solution over a 1 h period following 1 h of stabilization at 10 (±2) °C. The reversed osmotic flux from the phase-separated GE solution to the NaCl solution was similarly

calculated at 30 (±2) ℃.

3. Results and Discussion

3.1. Osmotic pressure in DEH/water mixtures

Although the concentration of the GEs could be known both in the homogeneous mixtures at low T and the water-rich phase at high T, the corresponding osmotic pressure is not directly proportional to the concentrations of the GEs. Therefore, the osmotic pressure of the DEH/water mixtures at various compositions was measured using two types of osmometers based on the depression of the freezing point and vapour pressure. The former was used for estimating osmotic pressures of homogeneous mixtures at low T near the freezing point, and the latter was used for estimating osmotic pressures of water-rich phase at high T with varying temperatures.

The osmotic pressure of homogeneous DEH/water solution at low T is shown in terms of osmolality in Fig. 2a. At low concentrations below 0.11 m, the osmolality was almost proportional to molality, which is a typical behavior of dilute solutions. However, the slope decreased drastically at intermediate concentrations. It represents the osmotic second virial coefficient (B in Eq. (1)) of the DEH/water mixtures is negative, and the DEH-DEH solute interaction is significantly high.[18] Then, the slope increased again, and 7.8 m DEH solution showed 3.0 Osm/Kg, which is around 3 times higher than that of seawater. The osmotic third virial coefficient (C in Eq. (1)) is positive, showing that higher

order interactions between solute molecules are significant at high concentrations.

The osmotic pressure of water-rich phase at high T is shown in Fig. 2b. The osmolality was almost proportional to molality at low concentrations, but it was saturated near the phase separation points. The decrease of the slope represents the solute-solute interaction increased as the concentration increased. LCST mixtures exhibit a certain constant vapour pressure with varying compositions in the phase-separated region because the compositions of the solvent-rich phase and the solute-rich phase are constant although their relative amounts are different. Therefore, I could reliably assume that the saturated value of the osmolality was close in value to the actual osmolality of the water-rich phase following phase separation at each temperature. The osmolality-molality relationship of DEH/water mixtures is quite similar to that of triethylamine (TEA)/water mixtures, a classical example of the LCST mixture.[19]

The saturated osmolality was inversely related to temperature. The saturated osmolalities of the DEH/water mixtures were 0.060, 0.050, and 0.045 Osm/kg at 30, 40, and 50 ° C, respectively. Because the concentrations of the water-rich phases of the phase-separated DEH/water mixtures at high T were also inversely related to temperature (Table 1), the decrease in the saturated osmolality was expected. Because the osmotic pressure of the water-rich phase determines the minimum salt concentration of the resulting water, as mentioned above, the lower osmolality of the

water-rich phase in the DEH/water mixtures is remarkably beneficial in reducing the final salt concentration. For example, the osmolality of the water-rich phase in the DEH/water mixtures at 30 ° C (0.060 Osm/kg) was similar to that of a 0.025 m NaCl solution; six times lower than physiological saline (0.15 m). Theoretically, an approximately 0.025 m NaCl solution can be produced from seawater (0.62 m NaCl equivalent) through a DEH-based FO system without any additional reverse osmotic pressure.

3.2. Osmotic water withdrawal and release

The osmotic water withdrawal from high-salt NaCl solutions at low T and the subsequent water release into low-salt NaCl solutions at high T were examined to demonstrate the feasibility of GEs as draw solutes in FO. Based on the phase diagrams of DEH, I selected low and high temperatures of 10 and 30 ° C, respectively.

Fig. 3a displays the osmotic water flux from NaCl solutions to the DEH draw solutions through a semipermeable membrane at 10 ° C expressed as litres per square meter per hour (L m^{-2} h^{-1}; LMH). Due to the miscibility of DEH with water at 10 ° C, the concentration of DEH could be freely selected. To make the process amenable to repeated cycling, I selected a DEH draw solution of 12 m (70 w/w %) because this value is the concentration of DEH in the solute-rich phase at 30 ° C (Table 1). The water flux toward the draw solution increased as the concentration gradient increased. The DEH draw solution was able to draw water from a seawater equivalent solution (0.62 m NaCl) with a flux of

0.62 LMH.

Fig. 3b depicts the osmotic water release from the water-rich phase into NaCl solutions at 30 ° C. The concentrations of the water-rich phases in the DEH mixtures at 30 ° C (0.081 m) were used as the operating concentrations for water release. The DEH water-rich phase was able to release water to a 0.15 m NaCl solution (equivalent to physiological saline). It was also able to release fresh water to even 0.050 m NaCl solutions. Comparing the osmolality of DEH with that of NaCl at 30 ° C (Fig. 2b and 4), the water release from the water-rich phase into the low-salt NaCl solution was quite satisfactory.

3.3. Water production yield based on the phase diagram and selection of ideal thermoresponsive draw solutions

Desalinated water production through the thermoresponsive osmotic system can be estimated based on the phase diagram of the draw solution (Fig. 5). For the recycling, I would start from the draw solution with the concentration of C_s, the concentration of the solute-rich phase at T_{high}. The drawing solution is diluted through the drawing process. At the maximum dilution, the concentration would finally reach to C_{eq}, the concentration with an equal osmotic pressure with the feed solution. Then, the diluted draw solution is heated to T_{high}, and the solution was phase-separated into two phases, a solute-rich phase with a concentration of C_s and a water-

rich phase with a concentration of C_w. The relative ratio between the solute-rich phase and the water-rich phase is amount of two phases is α:β, from the lever rule.[20] Water molecules in the water-rich phase are osmotically transferred to mild saline. As water is released, the amount of water-rich phase is decreased gradually. In this step, C_w and C_s are maintained and only the relative ratio between two phases changes to α':β'. The amount of the solute-rich phase increases, while the amount of the water-rich phase decreases. Finally, the solute-rich phase can be re-used as a draw solution for the second cycle after cooling to T_{low}.

For the drawing from the feed solution, C_{eq} should be lower than C_s. Also, the dilution below C_w is meaningless because the drawing solution cannot be phase-separated at T_{high} ($C_w < C_{eq} < C_s$). For the water release, the osmotic pressure of C_w should be lower than the osmotic pressure of the mild saline. Therefore, the minimum concentration of the product water is determined by the C_w.

Through the whole cycle, I could obtain a low-salt solution equivalent to a C_w-draw solution from a high-salt solution equivalent to a C_{eq}-draw solution. If the difference between C_{eq} and C_w is large, I can obtain a much diluted product water, but at the same time, the amount of product water becomes small due to the high α:β ratio. Reversely, if difference between C_{eq} and C_w is small, I can obtain a large amount of product water due to the low α:β ratio, but the dilution factor should be small. Therefore, I should choose an appropriate draw solute according to the objective.

Four important characteristics for an ideal thermoresponsive

draw solution can be partially predicted from the phase diagram: the maximum solubility or osmolality at low T, the phase separation temperature, the concentration (C_w) or osmolality of the water-rich phase at high T, and the concentration of the solute-rich phase at high T (C_s).

Because the maximum solubility or osmolality at low T determines the maximum drawable concentration of the feed solution, miscibility over a wide range of concentrations of DEH/water mixtures is highly valuable. In this study, a seawater equivalent saline was drawable using the DEH-based draw solutions.

The phase separation temperature determines the operating temperature gradient. Because the energy efficiency of an FO system is largely dependent on the operating temperature for separation (high T), the ability to conduct phase separation near room temperature is very attractive. In this study, 10 and 30 ° C were chosen as the low T and high T, temperatures which are readily achievable using sunlight-induced diurnal temperature changes or waste heat from factories or power plants.

As described above, C_w and C_s determines the minimum concentration and the amount of product water (or the α:β ratio). The solute-rich phase is recovered into the draw solution by circulation, and the water-rich phase releases water into the product water through a semipermeable membrane. The lower the C_w, the lower the concentration of the final product water *via* spontaneous osmosis. The higher the C_s, the larger the amount of

the product water due to the low α:β ratio.

In this study, an approximately 0.050 m NaCl solution was readily obtained from the water-rich phase by spontaneous osmosis from a seawater equivalent. It is expected that fresh water-grade salt solutions (<0.010 m) can be obtained using this method given the future discovery of thermoresponsive materials with lower residual concentrations in the water-rich phase (*i.e.*, exhibiting C_w that are much closer to the *y*-axis). Of course, final product water with a much lower salt concentration can be obtained by other methods, including reverse osmosis (RO). Because the osmotic pressure of the water-rich phase of the DEH/water mixtures at 30 ° C is approximately 1.6 atm, the RO process can produce fresh water at much lower operating pressures compared with the pressures required in direct RO from seawater (>27 atm). In addition, larger amount of water can be obtained per each cycle using temperature sensitive materials with a low α:β ratio from higher C_s.

Razmjou *et al.* reported that energy requirement for the recovery of water-swollen PNIPAAM hydrogel having swelling ratio of 5 will be in range of 1.12-3.57 kWh/m^3 considering the heat of transition of the hydrogel.[22] Since the operation temperature was below those used in the report, the presented FO methods in my research would require similar degree of minimum energy consumption assuming that heat of LCST transition of the draw solutes is in a similar level.

4. Conclusions

To overcome the limitations of current FO desalination systems based on liquid–gas phase separation, I developed a FO control based on the LCST liquid–liquid phase separation of GEs by mild temperature changes. Water was drawn from a seawater equivalent at 10 ° C and released into a low–salt saline (approximately 0.05 m) at 30 ° C using the GE–based draw solutions. The phase diagram–based approach will be helpful in the future development of ideal draw solutes with high solubilities at low T, mild phase transition temperatures, low C_w and high C_s. Practical FO desalination can be achieved in the near future with the development of various draw solutes and advanced membranes exhibiting higher water flux and higher rejection.[21]

5. References

[1] J. F. Reynolds, D. M. Stafford Smith, E. F. Lambin, B. L. Turner, M. Mortimore, S. P. J. Batterbury, T. E. Downing, H. Dowlatabadi, R. J. Fernandez, J. E. Herrick, E. Huber-Sannwald, H. Jiang, R. Leemans, T. Lynam, F. T. Maestre, M. Ayarza and B. Walker, *Science*, 2007, 316, 847; C. J. Vörösmarty, P. B. McIntyre, M. O. Gessner, D. Dudgeon, A. Prusevich, P. Green, S. Glidden, S. E. Bunn, C. A. Sullivan, C. Reidy Liermann and P. M. Davies, *Nature*, 2010, 467, 555.

[2] R. F. Service, Science, 2006, 313, 1088; Q. Schiermeier, *Nature*, 2008, 452, 260; M. Elimelech and W. A. Phillip, *Science*, 2011, 333, 712.

[3] R. E. Karavath and J. A. Davis, Desalination, 1975, 16, 151; T. Y. Cath, A. E. Childress and M. Elimelech, *J. Membr. Sci*, 2006, 281, 70; D. Li and H. Wang, *J. Mater. Chem. A*, 2013, 1, 14049; Q. Ge, M. Ling, T.-S. Chung, *J. Memb. Sci.,* 2013, 442, 225.

[4] J. R. McCutcheon, R. L. McGinnis and M. Elimelech, *Desalination*, 2005, 174, 1; J. R. McCutcheon, R. L. McGinnis and M. Elimelech, *J. Membr. Sci.*, 2006, 278, 114.

[5] R. L. McGinnis, N. T. Hancock, M. S. Nowosielski-Slepowron, G. D. McGurgan, *Desalination*, 2013, 312, 67; N. T. Hancock, Engineered Osmosis for Energy Efficient Separations: Optimizing Waste Heat Utilization FINAL SCIENTIFIC REPORT DOE F 241.3 DE-EE0003467, 2013; J. E. Miller, L. R. Evans, Sandia Report, SAND2006-4634, Sandia National Laboratories, California, 2006; R. Wang, L. Shi, C.Y.Y. Tang, S.R. Chou, C. Qiu and A.G. Fane*, J. Membr. Sci.,* 2010, 355, 158; N. Ma, J. Wei, R. Liao and C. Y. Tang, *J. Membr. Sci.,* 2012, 405-406, 149.

[6] N. Y. Yip, A. Tiraferri, W. A. Phillip , J. D. Schiffman and M. Elimelech, *Environ. Sci. Technol.,* 2010, 44, 3812.

[7] Z. Liu, H. Bai, J. Lee and D. D. Sun, *Energy Environ. Sci.,* 2011, 4, 2582.
[8] M. M. Ling, K. Y. Wang, and T.-S. Chung, *Ind. Eng. Chem. Res.,* 2010, 49, 5869.
[9] D. Li, X. Zhang, J. Yao, Y. Zeng, G. P. Simonb and H. Wang, *Soft Matter,* 2011, 7, 10048; D. Li, X. Zhang, J. Yao, G. P. Simonb and H. Wang, *Chem. Commun*., 2011, 47, 1710.
[10] R. B. Griffiths and J. C. Wheeler, *Phys. Rev. A*, 1970, 2, 1047.
[11] H. Kim, S. Lee, M. Noh, S. H. Lee, Y. Mok, G. Jin, J.-H. Seo and Y. Lee, *Polymer*, 2011, 52, 1367.
[12] P. G. Jessop, S. M. Mercera and D. J. Heldebrant, *Energy Environ. Sci.,* 2012, 5, 7240; M. L. Stone, C. Rae, F. F. Stewart and A. D. Wilson, *Desalination*, 2013, 312, 124.
[13] M. Noh, Y. Mok, S. Lee, H. Kim, S. H. Lee, G. Jin, J.-H. Seo, H. Koo, T. H. Park and Y. Lee, *Chem. Commun*., 2012,48, 3845.
[14] S. P. Christensen, F. A. Donate, T. C. Frank, R. J. LaTulip and L. C. Wilson*, J. Chem. Eng. Data*, 2005, 50, 869.
[15] X.-X. Li, W.-D. Zhou, X.-Y. Li, J.-L. Sun and Wei Jiang, *J. Mol. Liq.* 2009, 148, 73.
[16] Y. Mok, D. Nakayama, M. Noh, S. Jang, T. Kim and Y. Lee, *Phys. Chem. Chem. Phys*., 2013, 15, 19510.
[17] T. Y. Cath, M. Elimelech, J. R. McCutcheon, R. L. McGinnis, A. Achilli, D. Anastasio, A. R. Brady, A. E. Childress, I. V. Farr, N. T. Hancock, J. Lampi, L. D. Nghiem, M. Xie, N. Y. Yip, *Desalination*, 2013, 312, 31.
[18] J.-P. Simonin, *J. Phys. Chem. B*, 2001, 105, 5262.
[19] L. D. Roberts and J. E. Mayer, *J. Chem. Phys*., 1941, 9, 852.
[20] D. A. McQuarrie and J. D. Simon, in Physical Chemistry: a molecular approach, University Science Books, Sausalito, 1997, ch.24, pp. 970-977.
[21] M. Kumar, M. Grzelakowski, J. Zilles, M. Clark and W. Meier, *Proc. Natl. Acad. Sci. U.S.A.,* 2007, 104, 20719; H. G. Park, F. Fornasiero, J. K. Holt, C. P. Grigoropoulos and O. Bakajin,

Nano Today, 2007, 2, 22.; M.T. M. Pendergast and E. M.V. Hoek, *Energy Environ. Sci.*, 2011, 4, 1946.; X. Song , Z. Liu and D. D. Sun*, Adv. Mater.*, 2011, 23, 3256.; D. Cohen－Tanugi and J. C. Grossman, *Nano Lett.*, 2012, 12, 3602.

[22] A. Razmjou, Q. Liu, G. P. Simon, and H. Wang, *Environ. Sci. Technol.*, 2013, 47, 13160.

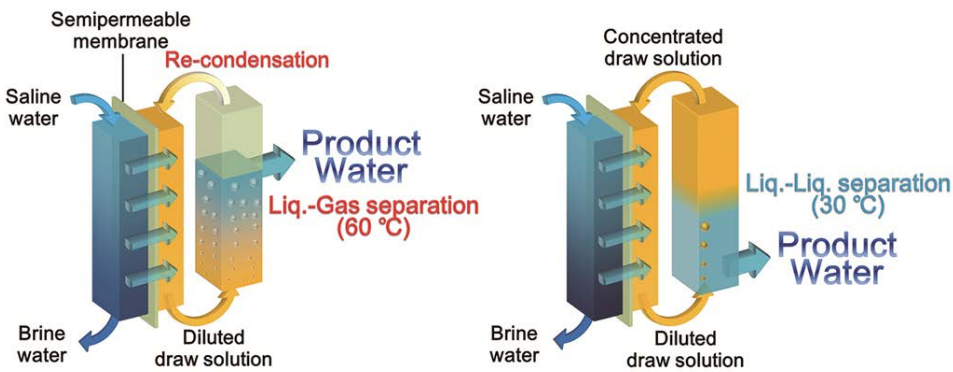

Figure 1. Schemetic illustration of the FO desalination systems based on a liquid–gas phase separation (left) and a liquid–liquid phase separation (right).

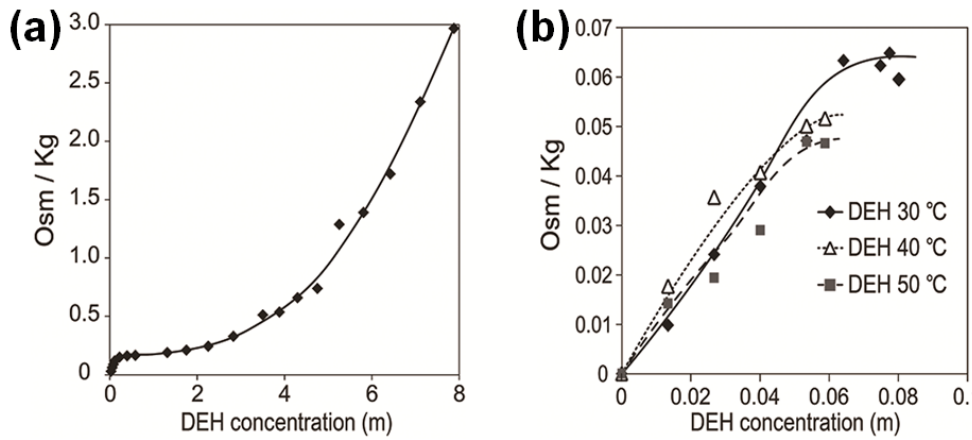

Figure 2. Osmolality of DEH/water mixture at various concentrations (a) at low T measured by freezing point depression and (b) at high T measured by vapor pressure depression.

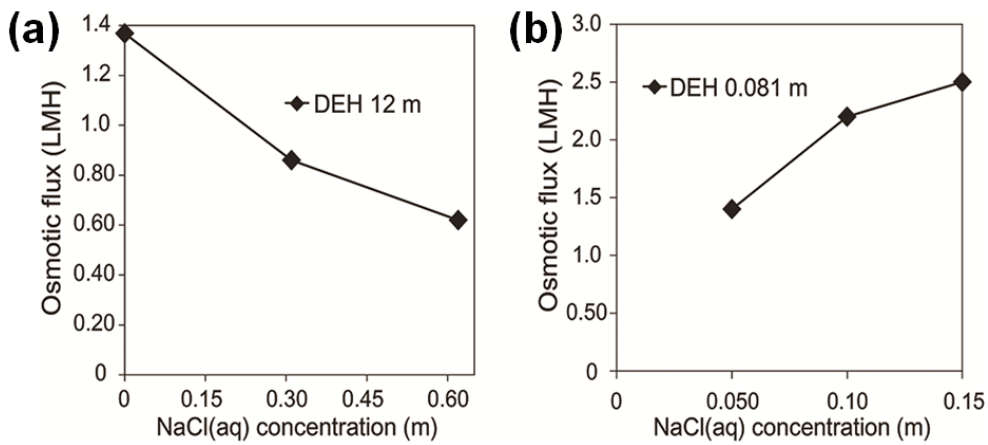

Figure 3. Osmotic flux between the DEH aqeous solution and NaCl solutions at (a) 10 and (b) 30 ° C. (a) The flow from the NaCl solution to a12 m DEH solution. (b) The flow from the 0.081 m DEH solution (*i.e.*, water-rich phase) to the NaCl solution.

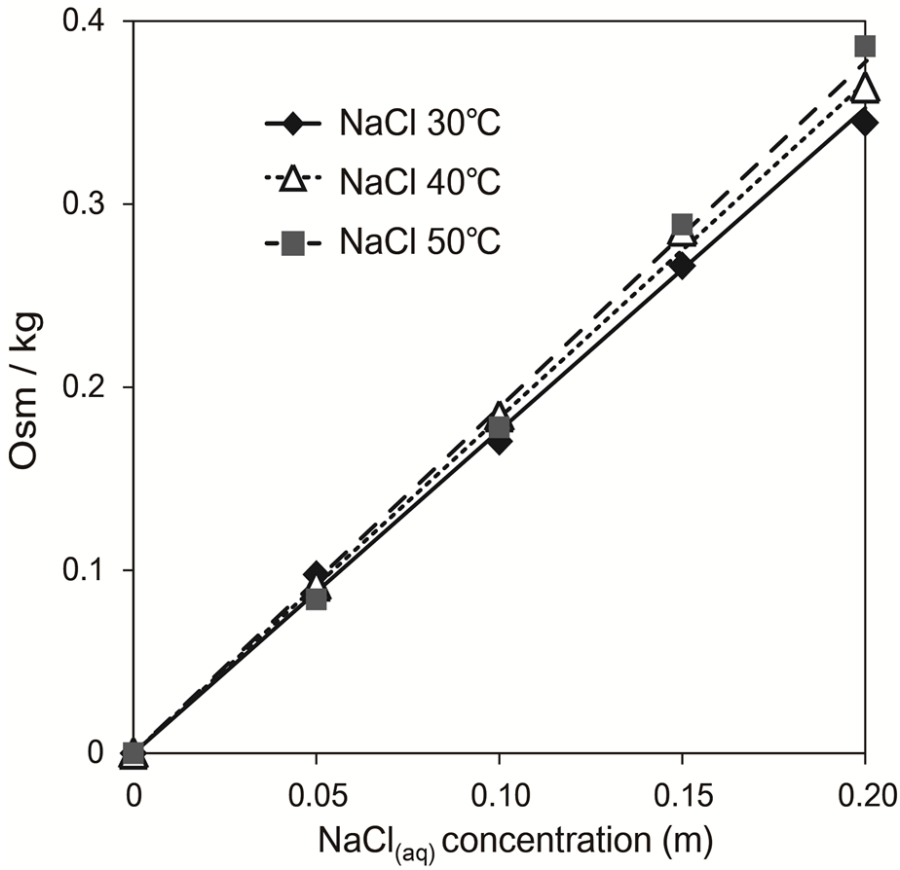

Figure 4. Osmolality of $NaCl_{(aq)}$ solution

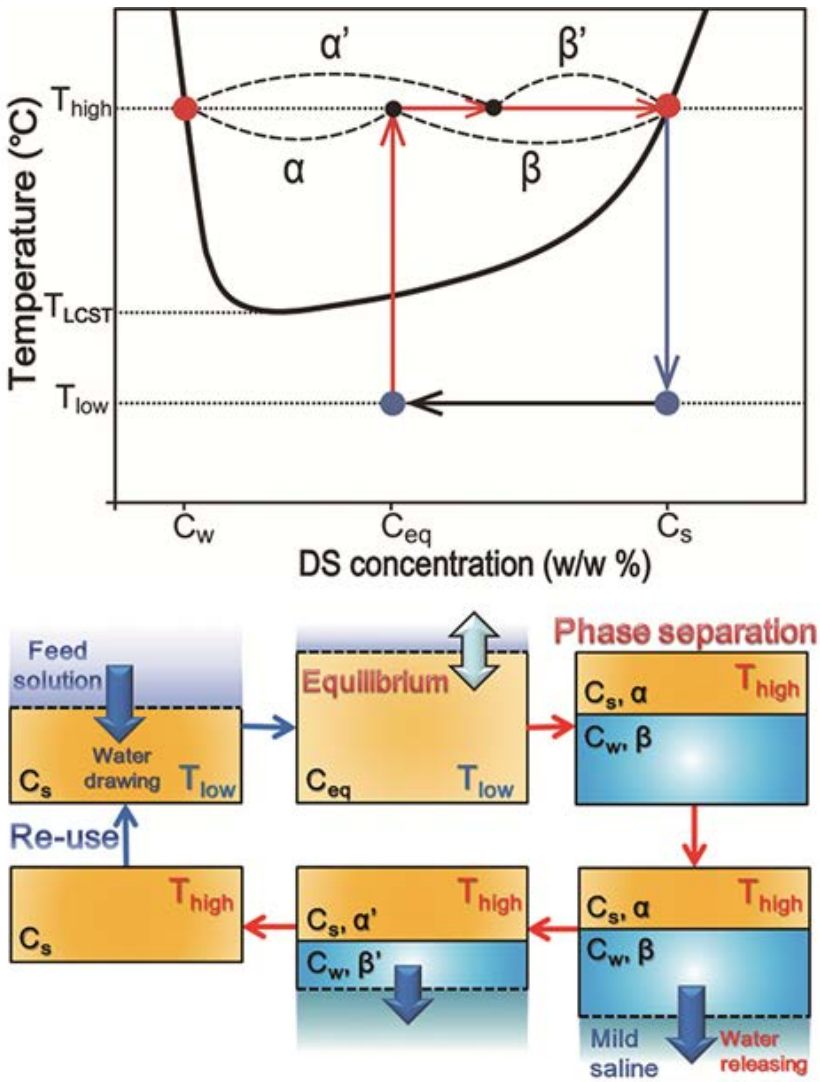

Figure 5. Illustration of a FO desaliation process by a phase diagram and a schematic diagram describing relative concentrations and amounts of each phase. DS: draw solute; T_{LCST}: LCST temperature; T_{high} and T_{low}: operation temperatures (high T and low T); C_s: the DS concentration in the draw solute-rich phase after phase separation at T_{high}; C_w: the DS concentration in the water-rich phase after phase separation at T_{high}; C_{eq}: the DS concentration of draw solution with an equivalent osmotic pressure to the feed solution.

Table 1 The GE concentration in each phase after the phase separation

		GE concentrations after phase separation (w/w%/m)					
		30 °C		40 °C		50 °C	
Draw solutes		PD[a]	NMR[b]	PD	NMR	PD	NMR
Water-rich phase	DEH	1.5/0.079	1.5/0.081	1.1/0.059	1.1/0.059	0.93/0.049	1.1/0.056
	DPP	16/1.1	13/0.82	9.9/0.63	8.3/0.51	7.3/0.45	7.5/0.46
	PB	5.0/0.40	4.7/0.37	3.9/0.30	3.7/0.29	3.6/0.28	3.4/0.27
GE-rich phase	DEH	53/5.8	70/12	62/8.4	75/16	67/11	79/19
	DPP	81/24	77/19	84/29	79/21	85/33	79/22
	PB	86/46	88/53	87/49	89/60	87/49	91/77

[a] Concentrations based on the phase diagram. [b] Concentrations measured by ^{1}H-NMR in GE–D_2O mixtures.

Table 1. The GE concentration in each phase after the phase separation.

List of Publications

1. Heejin Kim, Seonju Lee, Minwoo Noh, So Hyun Lee, Yeongbong Mok, Geun-woo Jin, Ji-Hun Seo, and Yan Lee, Thermosensitivity Control of Polyethylenimine by Simple Acylation, Polymer, 52(6), 1367-1374 (2011)

2. Minwoo Noh, Yeongbong Mok, Seonju Lee, Heejin Kim, So Hyun Lee, Geun-woo Jin, Ji-Hun Seo, Heebeom Koo, Tae Ha Park, and Yan Lee, Novel Lower Critical Solution Temperature Phase Transition Materials Effectively Control Osmosis by Mild Temperature Changes, Chemical Communications, 48(32), 3845-3847 (2012)

3. Sangmok Jang, Seonju Lee, Heejin Kim, Jiyeon Ham, Ji-Hun Seo, Yeongbong Mok, Minwoo Noh, and Yan Lee, Preparation of pH-Sensitive CaP Nanoparticles Coated with a Phosphate-based Block Copolymer for Efficient Gene Delivery, Polymer, 53(21), 4678-4685 (2012)

4. Minwoo Noh, Yeongbong Mok, Daichi Nakayama, Sangmok Jang, Seonju Lee, Taeho Kim, and Yan Lee, Introduction of pH-Sensitive Upper Critical Solution Temperature (UCST) Properties into Branched Polyethylenimine, Polymer, 54(20), 5338-5344 (2013)

5. Yeongbong Mok, Daichi Nakayama, Minwoo Noh, Sangmok Jang, Taeho Kim, and Yan Lee, Circulatory Osmotic Desalination Driven by a Mild Temperature Gradient Based on Lower Critical Solution Temperature (LCST) Phase Transition Materials, Physical Chemistry Chemical Physics, 15(44), 19510-19517 (2013)

6. Daichi Nakayama, Yeongbong Mok, Minwoo Noh, Jeongseon Park, Sunyoung Kang, and Yan Lee, Lower Critical Solution Temperature (LCST) Phase Separation of Glycol Ethers for Forward Osmotic Control, Physical Chemistry Chemical Physics, 16(11), 5319-5325 (2014)

7. Wonmin Choi, Sunyoung Kang, Yeongbong Mok, Euddeum Park, Youngjoon Song, Sojung Choi, and Yan Lee, Unlocking pH-Responsive Degradability of Fumaramic Acid Derivatives by Photoisomerization, Chemistry – A European Journal , 20(48), 15715-15718 (2014)

8. Minwoo Noh, Sunah Kang, Yeongbong Mok, So Jung Choi, Jeongseon Park, Jannick Kingma, Ji-Hun Seo, and Yan Lee, Upper Critical Solution Temperature (UCST) Phase Transition of Halide Salts of Branched Polyethylenimine and Methylated Branched Polyethylenimine in Aqueous Solutions, Chemical Communications, 52, 509-512 (2016)

9. Jeongseon Park, Minwoo Noh, Min Keun Chey, Yeongbong Mok, and Yan Lee, Control of Osmotic Pressure Through CO2-Capture and Release Facilitated by the Lower Critical Solution Temperature (LCST) Phase Transition of Acylated Branched Polyethyleneimine, RSC Advances, 6, 26526-26530 (2016)

10. Byeongho Lee, Kunzhou Li, Hong SikYoon, JeyongYoon, Yeongbong Mok, Yan Lee, Hong H. Lee and Yong Hyup Kim, Membrane of Functionalized Reduced Graphene Oxide Nanoplates with Angstrom-Level Channels, Scientific Reports, DOI: 10.1038/srep28052 (2016)

*Data in this thesis were previously described in the 'List of Publications' written above and also in the following two theses; 1) "Lower critical solution temperature (LCST) phase separation of glycol ethers for forward osmotic control" (Daichi Nakayama, 서울대학교 대학원, 2014) and 2) "Development of Thermo-Responsive Materials and Their Potential Application of Osmotic Control" (노민우, 서울대학교 대학원, 2016)

Abstract (국문초록)

신호 감응성 물질은 외부의 물리화학적 환경 변화에 의해 그 물성의 변모를 나타내는 물질로 신호에 의해 다른 특성을 나타내는 기능성 스마트소재의 기본 구성단위가 된다. 이러한 신호로서의 기능을 할 수 있는 요소는 온도, 빛, pH, 환원력, 전기장 등이 있으며 물리적 신호 중에서 온도 감응성은 그 물성 변모의 효과성과 신호 주입의 용이성으로 인해 가장 많은 연구가 진행되어 왔다. 온도 감응성 물질은 크게 저임계용해온도 (lower critical solution temperature; LCST) 또는 고임계용해온도 (upper critical solution temperature; UCST) 현상 중 하나의 특징을 갖는 물질로 온도 변화에 특이적으로 용해-상분리 간의 전환을 갖는 것을 주요한 특징으로 갖는다. 저임계용해온도 현상을 갖는 물질은 저온에서 용매에 잘 녹아 균일상을 이루다 특정 온도 이상에서 용매에 녹지 못해 상분리를 이루고 이와 반대로 고임계용해온도 현상의 물질은 고온에서 균일상을, 특정 온도 이하에서 상분리를 이루게 된다.

특히 수용액에서의 임계용해온도현상을 활용하여 조직공학, 약물전달 등과 같은 분야에서 다양한 스마트소재들이 개발되었다. 하지만 이러한 물질군들은 대부분 높은 수준의 분자량을 갖는 고분자 물질이 대부분인 것으로 밝혀져 있다. 이는 저분자량 물질의 경우 그것이 가지게 되는 높은 통계적 용해 엔트로피 (statistical entropy of mixing) 때문으로 이 양의 값을 갖는 엔트로피 변화량으로 인해 관찰 가능한 일반적인 온도범위에서 기존 온도 감응성 물질의 반복 단위를 갖는 저분자량 물질은 물에 쉽게 녹아버리게 된다. 이러한 특성으로 인해 온도 감응성 물질을 이용해 온도에 따른 큰 수준의 유효 몰농도 차이는 쉽게 보고되지 않았다. 또한 온도 감응성의 효율적 조절을 위한 방침으로 원격에서 제공되는 신호를 이용해 쉽게 온도감응성의 조절이

가능하다면 더욱 정밀하고 고차원적인 신호 감응성을 획득할 수 있을 것이다.

이에, 나는 본 학위논문에서 분자량을 낮추어도 저임계용해온도 현상을 가질 수 있는 온도 감응성 물질에 관한 연구를 첫 번째로 제시한다. 또한 기존 보고된 빛-온도 이원 감응성보다 효과적으로 빛 신호로 온도 감응성을 조절할 수 있는 방안을 제안한다. 끝으로 고농도 저분자량 온도 감응성 물질로 구현할 수 있는 현상에 관한 예시로 삼투현상의 조절을 다룬다.

다량의 아민을 함유한 고분자인 가지형 폴리에틸렌이민 (branched polyethylenimine; b-PEI)을 아실화하여 다양한 온도감응성 물질을 개발하였다. 나아가 위 아실화된 b-PEI의 핵심 구조를 따온 저분자량 물질에서도 온도 감응성이 유효하게 나타나는 것을 알 수 있었고 높은 농도에서도 온도 감응성이 나타남을 확인하였다. 저분자량 온도감응성 물질의 구조에 대한 확장으로 글라이콜이써 (glycol ethers)의 온도 감응 특성 역시 확인하였다.

나아가 빛에 의해 친수성-소수성 전환이 가능한 아조벤젠 (azobenzene)을 기 개발된 온도감응성 b-PEI 유도체에 도입하여 빛에 의해 임계용해온도 현상이 수용액에서 효율적으로 조절되는 것을 확인하였다. 특히 보고된 문헌보다 더욱 효과적인 빛에 의한 저임계용해온도 변환을 확인하였고 최초로 빛에 의한 수용해성 고임계용해온도의 전환이 구현되었다.

끝으로 저분자량 온도감응성 물질을 활용한 새로운 현상에 대한 보고로 온도에 따른 삼투현상의 조절을 최초의 사례로서 구현하였다. 개발된 저임계용해온도현상을 갖는 저분자량 온도 감응성 물질들은 낮은 온도에서 물에 녹아 높은 삼투압을 나타내었고, 고온에서 상분리가 되어 실질적 삼투압이 현저히 낮아져 고정된 삼투압을 갖는 염수를 반투막

사이에 두고 온도에 따라 삼투 현상의 흐름이 가역적으로 조절되는 것을 확인하였다. 이러한 삼투현상의 조절을 활용해 서로 다른 온도에서 온도 감응성 용액의 연결을 통해 고농도의 염수를 저농도의 염수로 치환시키는 순환식 삼투법을 고안하여 담수화 공정으로의 가능성을 제시하였다.

상기한 구현들을 통해 나는 본 학위논문이 온도 감응성 물질의 분자량 특성과 복합 신호감응성에 대한 현시점까지 보고된 학술적 이해를 확장시키고 나아가 새로운 현상으로서의 삼투 기반 담수화 연구의 학문 및 기술적 발전에 근간이 되는 자료로 활용되기를 희망한다.

Keywords: 온도 감응성, 저임계용해온도 현상, 고임계용해온도 현상, 아조벤젠, 삼투 현상, 해수 담수화
Student Number: 2010-23088